

DIPLOMARBEIT

**RANS simulation of methane combustion in a Low Swirl
Burner**

Autor:

Mathias Neumayer

Matrikel-No:

2968339

Betreuer:

Prof. Dr.-Ing. Thomas Sattelmayer

Dr. Christoph Hirsch

Prof. Philip Malte und Prof. John Kramlich

April 16, 2013

Erklärung

Hiermit versichere ich, die vorliegende Arbeit selbständig verfasst zu haben. Ich habe keine anderen Quellen und Hilfsmittel als die angegebenen verwendet.

Ort, Datum

Mathias Neumayer

Contents

Acknowledgment - Danksagung	5
Abstract - Zusammenfassung	6
Nomenclature	6
1 Introduction	8
1.1 Motivation	8
1.2 Literature review	8
2 Experiment Setup	10
2.1 General	10
2.2 Low Swirl Combustion	13
2.3 Flame regime	15
2.4 Turbulent flame speed	17
3 Simulations	19
3.1 Domain and mesh	19
3.2 Boundary conditions	19
3.3 Settings in Fluent	22
3.4 Combustion models	23
3.4.1 Eddy Dissipation Concept model	23
3.4.2 Turbulent Flame Speed Closure model	24
3.5 Stability and convergence of the simulation runs	25
4 Simulation results	26
4.1 Cold flow	26
4.2 Reacting flow	32
4.2.1 Plots of flame shape and position	32
4.2.2 Mesh independence study	40
4.2.3 Diagrams	41
5 Conclusion	45
A Appendix	46
A.1 Additional diagrams	46
A.2 Additional plots	47
A.3 Additional information	50

“Ich habe keine besondere Begabung, sondern bin nur leidenschaftlich neugierig.” (Albert Einstein)

Acknowledgment - Danksagung

Ich möchte mich ganz herzlich bei Professor Sattelmayer and Dr. Hirsch für die sehr gute Betreuung, während meiner Diplomarbeit, bedanken. Die sehr gute Lehre des Thermodynamik Lehrstuhls hat mich stark geprägt im Laufe meines Studiums. Die von Dr. Hirsch mit sehr viel Engagement gehaltene Vorlesung Verbrennung hat mich fasziniert, und bei mir das Bedürfnis geweckt, während meines Studiums, nochmal tiefer in das Thema Verbrennung einzusteigen.

I would like to thank Professor Malte and Professor Kramlich for giving me the opportunity to do this research project in the Combustion Research Group at University of Washington, in Seattle. I appreciated their support during my studies in combustion and my simulations. Their doors were always open, when I needed advice. I would also like to thank my colleagues Megan, Shaz and Igor, who generously shared their simulation knowledge and experience with me and cheered me up after my first series of crashed simulation runs.

Abstract - Zusammenfassung

In this research project, simulations of premixed lean methane flames in a Low Swirl Burner are conducted using the Software ANSYS Fluent 14.0. The results are compared with the corresponding experimental data. A 2-dimensional, axisymmetric, steady state, Reynolds-Averaged-Navier-Stokes (RANS) approach is used for the simulations. First, non-reacting simulations are performed. The comparison with the experimental data shows a good match. For the reacting simulations, two different combustion models are used, the Eddy-Dissipation-Concept (EDC) model and the Turbulent Flame Speed Closure (TFC) model. The results show that the EDC-combustion-model, which can incorporate detailed chemistry, is not able to predict the flame shape and position correctly, as it is seen in the experiments. In contrast, the TFC-combustion-model, modeling combustion without individual species, predicts the correct flame shape and position.

Diese Forschungsarbeit berichtet über die Simulation von magerer, vorgemischter Methanverbrennung in einem "Low Swirl Burner", mit dem Softwareprogramm ANSYS Fluent 14.0. Die Ergebnisse werden mit den Daten des zu Grunde liegenden Experiments verglichen. Die Simulationen sind 2-dimensional, axensymmetrisch und stationär, und verwenden die Reynolds-Averaged-Navier-Stokes (RANS) Lösungsmethode. Die reinen Strömungssimulationen zeigen gute Übereinstimmung mit den dazugehörigen Daten des Experiments. Um die Verbrennungsprozesse zu simulieren, werden zwei verschiedene Simulationsmodelle verwendet, das "Eddy-Dissipation-Concept" Modell, und das "Turbulent-Flame-Speed-Closure" Modell. Die Vergleiche zeigen, dass das EDC-Verbrennungsmodell, welches detaillierte Verbrennungsschemie berücksichtigt, nicht in der Lage ist die Form und Position der Flamme vorherzusagen, so wie es aus dem Experiment bekannt ist. Das TFC-Verbrennungsmodell dahingegen, schafft es die Form und Position der Flamme zu bestimmen.

Nomenclature

Symbol	Meaning	Unit
A_f	flame area	m^2
A_{ann}	area of annulus	m^2
A_{eff}	effective area of flow	m^2
A_{geo}	geometric area	m^2
A_{hole}	area of hole in perforated plate	m^2
A_{vane}	cross-sectional area of one vane	m^2
A_c	area of flow, center inlet	m^2
A_s	area of flow, swirl inlet	m^2
c	reaction progress variable	-
C	empirical constant	-
C_{loss}	loss coefficient (Bernoulli)	-
C_z	Zimont model constant	-
C_ξ	volume fraction constant	-
C_τ	time scale constant	-
Da	Damköhler number	-
F_c	mass flow fraction through center inlet	-
F_s	mass flow fraction through swirl inlet	-
h	heat transfer coefficient	$W/(m^2 K)$
l_t	turbulent length scale	mm
l_K	Kolmogorov length scale	mm
\dot{m}	mass flow (rate)	kg/s
\dot{m}_{LSI}	total mass flow through Low Swirl Injector (LSI)	kg/s
\dot{m}_c	mass flow through center of LSI	kg/s
\dot{m}_s	mass flow through swirl annulus of LSI	kg/s
N_{holes}	number of holes in perforates plate	25
N_{vanes}	number of vanes in swirl annulus	16

Symbol	Meaning	Unit
p	pressure	Pa
p_{op}	operating pressure	Pa
Δp_{LSI}	pressure loss over LSI	Pa
\dot{Q}	heat release of combustion	kW
Sc_t	turbulent Schmidt-number	-
S_N	swirl number	-
S_l	laminar flame speed	m/s
S_t	turbulent flame speed	m/s
$S_{t,LD}$	local displacement turbulent flame speed	m/s
r	radius	mm
R	injector radius ratio	-
R_c	center radius of injector	-
R_0	outer radius of injector	-
Re	Reynolds-number	-
\mathcal{R}_i	reaction rate of species i	s^{-1}
T	temperature	K
U	velocity in axial direction	m/s
U_0	bulk velocity in axial direction	m/s
u'	velocity fluctuation in axial direction	m/s
V	velocity in radial direction	m/s
\vec{v}	overall velocity vector	m/s
W	velocity in tangential direction	m/s
Y_i	species mass fraction	-
Y_i^*	fine scale species mass fraction	-
α	thermal diffusivity	m^2/s
α_{vanes}	swirl angle of vanes	$^\circ$
α_{flow}	swirl angle of flow	$^\circ$
δ_l	laminar flame thickness	mm
ϵ	turbulent eddy dissipation	m^2/s^3
μ	dynamic viscosity	Ns/m^2
ν	kinematic viscosity	m^2/s
ξ^*	length fraction of the fine scales	-
ρ	density	kg/m^3
ρ_u	unburned density	kg/m^3
τ_c	chemical time scale	s
τ_t	turbulent time scale	s
τ^*	EDC time scale	s

1 Introduction

1.1 Motivation

With renewable energy sources, like wind energy or photovoltaic energy, becoming more important for power production, the issue of consistent power delivery becomes more pressing. One approach to compensate for the intermittency of those sources, is to use gas turbines, which can respond quickly to load changes in the power grid. Standard practice for methane combustion in industrial applications, like gas turbines, is using High Swirl Injectors. This technology has some disadvantages, like high pressure loss. Therefore, a new technology, using Low Swirl Injectors, has been proposed. In recent years, this technology has been investigated experimentally and numerically, as described in the next section 1.2. But up to date, no Reynolds-Averaged-Navier-Stokes (RANS) simulation of Low Swirl Injectors has been published. The goal of this research project is to close this gap. First, the experiment on a Low Swirl Injector, conducted by D. Beerer, is introduced. Then, the corresponding simulation approach is given. Finally, the results using two different combustion models are presented, and the findings are discussed.

1.2 Literature review

Before the simulations were performed, literature research was undertaken. The results are presented in this section.

The simulations described in this thesis are based on the experiments conducted by David Beerer at University of California, Irvine. Detailed information about the experiments can be found in D. Beerer's PhD thesis "Combustion characteristics and performance of Low-Swirl Injectors with natural gas and alternative fuels at elevated pressures and temperatures", [3]. Beerer's work offers a description of the experiment setup, as well as information about the combustion theory of turbulent premixed flames. It also contains velocity, flashback and emissions measurements. With the help of that thesis as well as other documents about the experiment, the model for the simulations is built. The velocity measurements are used to validate and adapt the simulation settings in general, and in particular the inlet boundary conditions. Other data, like flame photos, are used to analyze the simulation results.

Another important paper that was found, is the "Effects of combustor geometry on the flow fields and flame properties of a Low-Swirl Injector", (Proceedings of ASME Turbo Expo 2008: Power for Land, Sea and Air GT2008) [4]. That Low Swirl Injector was developed at the Lawrence Berkeley National Laboratory by R. Cheng et al. The authors R. Cheng and D. Littlejohn, present measurements of the velocity field of a Low Swirl Injector at atmospheric pressure. The Low Swirl Injector used in their research was scaled down for the experiments

1.2 Literature review

conducted by D. Beerer. As the Low Swirl Injector used by R. Cheng et al. is larger, and the operating pressure was at 1 atmospheric pressure, in contrast to 4 atmospheric pressures in the simulations, it is not possible to compare the simulation results quantitatively. However, qualitative comparison is possible and helps to verify the flow field produced by the simulations. That research paper also offered a good description of the aerodynamic principles of the Low Swirl Injector.

R. Cheng et al. also published a paper with the title “A combined computational and experimental characterization of lean premixed turbulent low swirl laboratory flames. I. Methane flames.” [6] It includes experimental data of the Low Swirl Injector developed at the Lawrence Berkeley National Laboratory by R. Cheng, and also simulation results. The researchers conducted 3-dimensional, transient simulations using a “low Mach number adaptive mesh refinement code (LMC)”. Their experience is used to compare the turbulence parameters at the inlet boundary conditions.

On the same Low Swirl Injector, running on methane and methane-hydrogen blends, 3-dimensional, transient, Large Eddy Simulations (LES) were conducted. The results can be found in the paper “Enabling advanced modeling and simulations for fuel-flexible combustors”, by H. Pitsch at Stanford University, published in 2010. [11] It includes data about the flow field, plots of the progress variable and temperature plots. Those are used to do qualitative comparison of the flow field, in particular the velocity and turbulence parameters, with the simulations conducted in this project. Additionally, information can be found about the stability and characteristics of the flow field in Low Swirl Combustion, which is helpful for comparison.

Two interesting theses from the Norwegian University of Science and Technology were found during the online literature research. The first one is a PhD thesis by O. Spangelo submitted in 2004, with the title “Experimental and theoretical studies of a low NO_x swirl burner.” [12] The second one is a Master’s thesis by A. Fiskum, with the title “Calculation of NO_x Formation in a Swirl Burner” submitted in 2008. [7] In both theses, simulations of the same High Swirl Injector running on methane and propane were carried out. In the master’s thesis, simulations with a different model and settings were carried out, using the experience of the PhD thesis. That High Swirl Injector has a different design, higher swirl numbers and the mixing of fuel and oxidizer happens downstream of the swirl vanes. O. Spangelo conducted 2-dimensional, steady state, Reynolds Averaged Navier Stokes-(RANS) simulations using the software Fluent. He compared three different turbulence models, and three different chemistry models offered in the Fluent version of 2003. Even though, the setup of those experiments and simulations were different, important information about mesh size, turbulence and chemistry models in Fluent can be obtained, as well as other valuable experience about 2-dimensional, steady state, RANS simulations.

2 Experiment Setup

2.1 General

In this section, the combustion experiment, conducted and published by D. Beerer at the University of California in Irvine, is described to the detail necessary for the numerical setup and the discussion. More detailed information can be found in D. Beerer's PhD thesis [3]. Beerer's work included experiments of lean premixed combustion of methane and methane and hydrogen blends (90% hydrogen and 10% methane) at elevated pressures. Particular interest was in the velocity field close to the flame anchoring point and the emissions, particularly CO and NOx. The down fired experiment setup consists of a premixer and a combustion chamber, which is divided into two parts, see figure 2.1. The first part is a quartz tube that is optically accessible for the Laser Doppler Velocimetry (LDV) measurements. The second part is a non-transparent steel tube, at the end of which, the emissions measurements were taken.

2.1 General

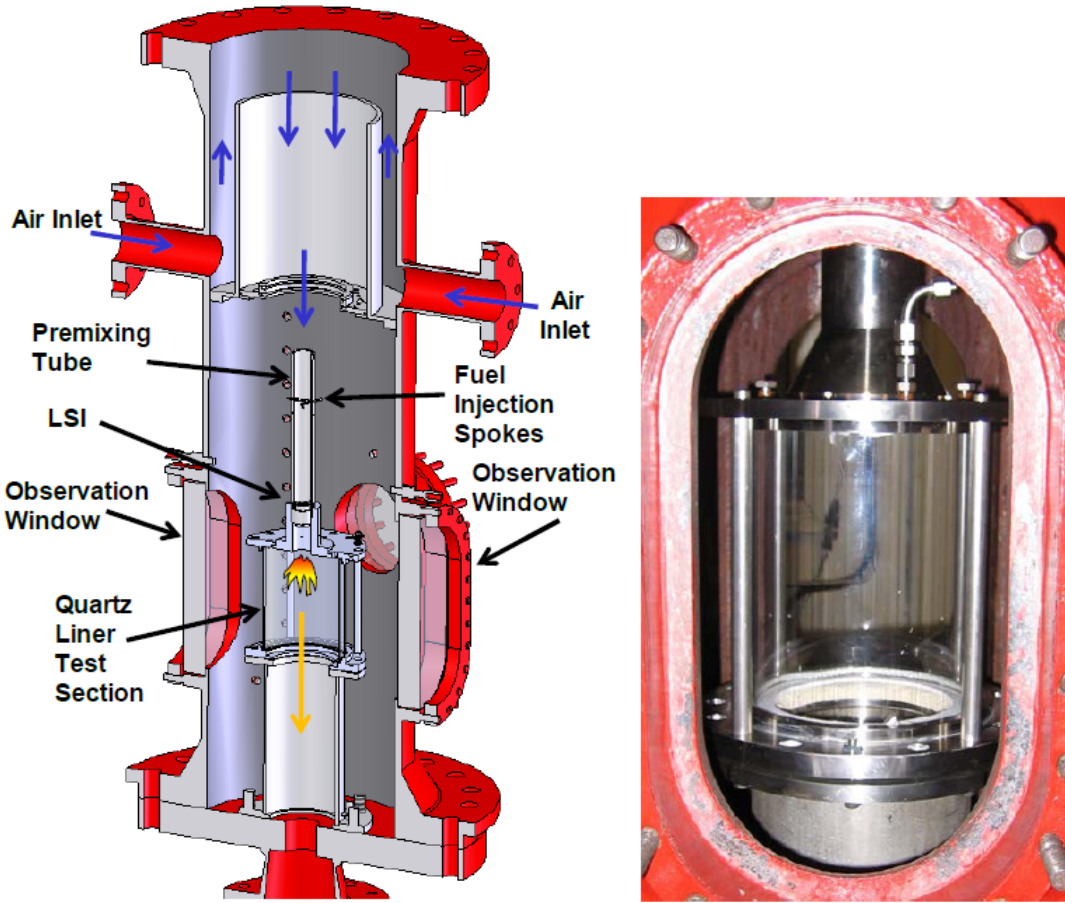


Figure 2.1: Cross section of the pressure vessel and combustor test section (left); photograph of test section through a window port (right). Figure 4-13 in [3]

After the premixer, the fuel air mixture flows through the Low Swirl Injector (LSI), and then into the combustion chamber. In figure 2.2 the Low Swirl Injector, the sudden expansion and the combustion chamber can be seen. The details of the Low Swirl Injector are explained in Chapter 2.2.

2.1 General

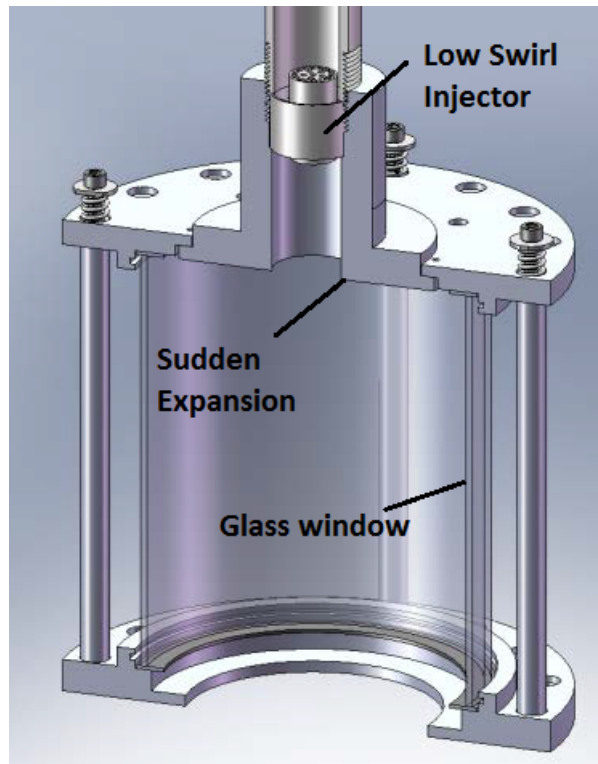


Figure 2.2: First part of the combustion chamber. Modified figure 4-14 from [3]

Out of the multiple experiment runs, conducted by D. Beerer, one is chosen for the simulations. (It is labeled “C-7” in D. Beerer’s PhD thesis [3]). The most important parameters, for that specific experiment run, can be found in the following Table 2.1. The adiabatic flame temperature is calculated with a program [1] from the Chair of Thermodynamics at Technical University of Munich. This program calculates the adiabatic flame temperature and product species mass fractions at equilibrium for combustion, in this case for pure methane.

Parameter	Symbol	Value	Unit
Fuel	CH_4	100	%
Heat release of combustion	\dot{Q}	387	kW
Operating pressure	p_{op}	416136	Pa
Equivalence ratio	Φ	0.71	-
Inlet temperature of fuel-air mixture	T_{in}	418	K
Adiabatic flame temperature	T_{ad}	1950	K
Total mass flow rate	\dot{m}_{tot}	0.194	kg/s

Table 2.1: Conditions of the experiment run, conducted by David Beerer, chosen for the simulations

2.2 Low Swirl Combustion

The Low Swirl Injectors, used for the experiment were developed by R. Cheng et al. at the Lawrence Berkeley National Laboratory. More detailed information can be found in D. Beerer's PhD thesis [3] or a paper by R. Cheng et al. [4]. Low Swirl flames are also suitable for research, because the flame can be simplified as a one-dimensional problem.



Figure 2.3: Low Swirl Injector. Right side inlet, left side outlet. [3]

The LSI consists of two regions. The flow in the outer region is swirled, that means the flow velocity has an axial and a tangential component. The tangential velocity component is produced by 16 swirl vanes, with an outlet angle $\alpha_{vanes} = 37^\circ$ to the axial direction, see Figure 2.3. The velocity in the inner region only has an axial component. The inner flow passes through a perforated plate (25 holes of 2.6mm diameter), which increases the turbulence. This is different than High Swirl Injectors, where the center is completely blocked, so all the incoming fluid is swirled. In the Low Swirl Injector, the supply of unswirled reactants through the center retards the formation of a Central Recirculation Zone (CRZ) and promotes flow divergence [4]. As the LSI consists of two regions, the center region (unswirled) and the outer region (swirled), the mass flow divides when going through it. This mass flow split can be changed by modifying the blockage ratio of the perforated plate in the center region. Changing the mass flow split influences the divergence rate and therefore the position of the flame. For example: If less mass flow is going through the center region (e.g. higher blockage ratio), the flow diverges more entering the combustion chamber. Then, the axial velocity decay on centerline is steeper and the flame position is closer to the dump plane.

Swirl can be quantified by the Swirl number S_N , representing the ratio of azimuthal momentum of the flow to the axial momentum. For the Low Swirl Injector a formula for the Swirl Number S_N can be found in [4]

$$S_N = \frac{2}{3} \tan(\alpha_{vanes}) \frac{1 - R^3}{1 - R^2 + [m_{LSI}^2 (\frac{1}{R^2} - 1)^2] R^2} \quad (2.1)$$

2.2 Low Swirl Combustion

$$R = \frac{R_c}{R_0} \quad (2.2)$$

$$m_{LSI} = \frac{\dot{m}_c}{\dot{m}_s} \quad (2.3)$$

where α_{vanes} is the swirl angle, R the ratio of the center channel radius, R_c to injector radius, R_0 and m_{LSI} the mass flow ratio of the mass flow through the center channel \dot{m}_c to the mass flow through the swirl annulus \dot{m}_s .

In High Swirl Injectors, strong recirculation zones are present, in the outer regions of the combustion chamber, as well as a recirculation zone in the center of the flow field. In those recirculation zones, hot reaction products, including radicals are transported back upstream, where they ignite the unburned fuel air mixture. With this effect, the flame is stabilized close to the High Swirl Injector.

In Low Swirl Injectors the axial momentum is greater than the azimuthal momentum, which results in swirl numbers smaller than unity. The calculated swirl number in this research is $S = 0.5$. The location where the flame is stabilized is called the lift off height x_f . In High Swirl Injectors, the flame is anchored at the inlet walls. In the case of the Low Swirl Injector, the flame can freely propagate downstream and it is stabilized where the Turbulent Flame Speed S_t is equal, but opposite to the mean velocity in the flow field. The flame appears lifted from the inlet nozzle. Therefore, it is a very important design criterion to match the flow field velocities to the Turbulent Flame Speed.

When the flow enters the combustion chamber, there is a jump in diameter, called sudden expansion. The radial momentum of the swirl makes the outer and the inner flow diverge. Because of the conservation of mass law, the mean axial velocity decreases with distance away from the sudden expansion. Close to the centerline, the velocity decay is linear. In the reacting case, the flame sits where the mean axial velocity is equal, but opposite to the turbulent flame speed. When the flow from the injector enters the combustion chamber, there is also a shear layer formed, between the incoming flow and the fluid that is already in the combustion chamber. Figure 2.4 shows the schematic flow field produced by the Low Swirl Injector.

2.3 Flame regime

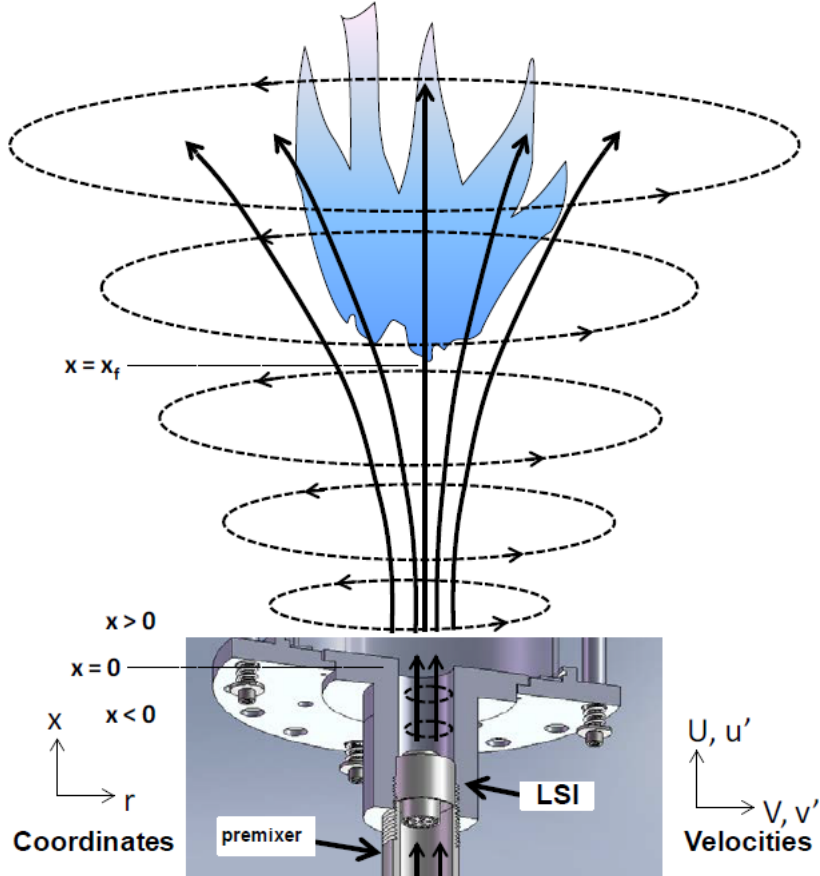


Figure 2.4: Flow field of Low Swirl Injector [3]

2.3 Flame regime

The flame regime for the simulated experiment is the “flamelets in eddies” regime, or “thin reaction zone” regime. It can be characterized by Damköhler numbers of approximately unity. The Damköhler number is defined as the ratio of the characteristic flow time τ_t to the characteristic chemical time τ_c

$$Da = \frac{\tau_t}{\tau_c} = \frac{\frac{l_t}{u'}}{\frac{\delta_l}{S_l}} \quad (2.4)$$

where l_t is the turbulent length scale, u' the velocity fluctuation, δ_l the flame front thickness, and S_l the laminar flame speed. In the flamelets in eddies regime, the characteristic flow time or turbulent time scale is on the same order as the characteristic times of the chemical reactions. Additionally, the flow field shows high turbulence intensities, which means the velocity fluctuation u' is significantly larger than the laminar flame speed S_l ($u'/S_l \gg 1$).

The turbulent Reynolds number is a measure of the inertial forces to the friction forces of the flow. ν is the kinematic viscosity.

2.3 Flame regime

$$Re_t = \frac{u' l_t}{\nu} = \frac{u' l_t}{S_l \delta_l} \quad (2.5)$$

Another criterion for this regime is the flame front thickness δ_l being larger than the Kolmogorov length scales l_K , but smaller than the largest eddies in the turbulent flow field l_t ($l_t > \delta_l > l_K$). This regime is characterized by Karlovitz numbers greater than unity.

$$Ka = \frac{\delta_l}{l_K} = \frac{(Re_t)^{\frac{1}{2}}}{Da} \quad (2.6)$$

The numeric values for the turbulence parameters are extracted from David Beerer's PhD thesis [3]. The values for the simulated case are given in Table 2.2. u' was measured with Laser Doppler Velocimetry (LDV) at the flame anchoring point during the experiment, and l_t was determined by performing an autocorrelation of the LDV data. δ_l was calculated with a mechanism developed by Davis et al. at USC. S_l was calculated with the software CHEMKIN.

Parameter	l_t	u'	δ_l	S_l	$\frac{u'}{S_l}$	$\frac{l_t}{\delta_l}$
Value	3mm	5.86m/s	0.19mm	0.23m/s	25.4	15.8

Parameter	τ_t	τ_c	Re_t	Da	Ka
Value	0.51ms	0.82ms	402	0.62	31.4

Table 2.2: Turbulence and flame regime parameters of simulated experiment run [3]

2.4 Turbulent flame speed

Figure 2.5 shows the flame regime diagram by Peters. The simulated experiment run is in the “Thin-Reaction Zone” flame regime (red dot).

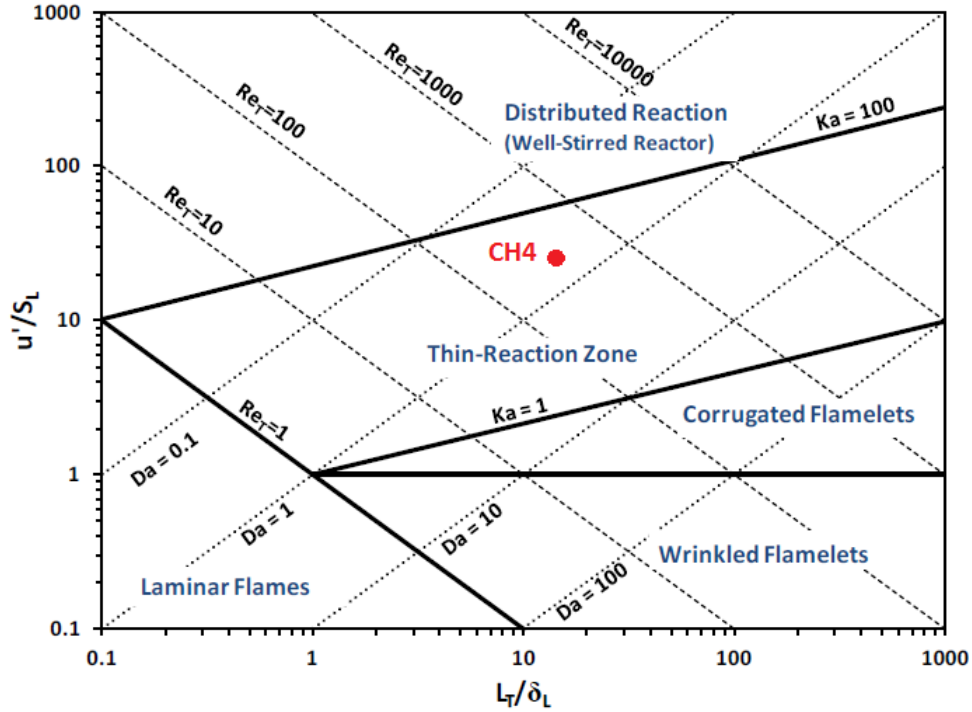


Figure 2.5: Regime diagram for premixed turbulent flames, Peters (2000). The red dot represents the simulated experiment run.

2.4 Turbulent flame speed

The laminar flame speed is only dependent on the thermal and chemical properties of the fuel air mixture, like temperature, pressure, equivalence ratio and the type of fuel. The turbulent flame speed depends on the mixture properties and on the characteristics of the flow field. In the book “An Introduction to Combustion” by Stephen Turns [13] in chapter 12, a good description of the turbulent flame speed can be found. For an observer traveling with the flame front, the turbulent flame speed can be defined as the velocity at which unburnt reactants enter the flame front, in the normal direction. With the conservation of mass law the turbulent flame speed can be expressed as

$$S_t = \frac{\dot{m}}{A_f \rho_u} \quad (2.7)$$

where \dot{m} is the mass flow rate of the reactants, ρ_u is the density of the unburned mixture, and A_f the time averaged area of the flame. In reality, the flame front in turbulent flames is wildly fluctuating, due to the turbulence, which makes it hard, sometimes impossible to measure. For this reason, other definitions of the turbulent flame speed were developed, using variables that can be measured in experiments.

2.4 Turbulent flame speed

For the wrinkled laminar flame regime Damköhler developed the following equation 2.8 for the turbulent flame speed.

$$\frac{S_t}{S_l} = 1 + \frac{u'}{S_l} \quad (2.8)$$

or

$$S_t = S_l + u' \quad (2.9)$$

In equation 2.9 the turbulent flame speed is linearly proportional to the turbulence intensity u' . In contrast to the laminar flame speed S_l , the turbulence intensity u' is strongly dependent on the turbulence in the flow field.

In the PhD Thesis of D. Beerer [3] two definitions can be found. The first is the (turbulent) Consumption Flame Speed $S_{t,C}$, which can be quantified by the rate at which the flame consumes reactants. The second is the (turbulent) Displacement Flame Speed $S_{t,D}$, which can be quantified by how quickly the flame moves through the flow. Both can be determined at either a specific point on the flame front (local), or averaged over the whole flame front (global). Investigations on Low Swirl Flames by Cheng and Sheperd [3] revealed that the Local Displacement Flame Speed is often two to three times higher than the Global Consumption Flame Speed. In Low Swirl Burners, the local displacement flame speed is the most relevant definition used. D. Beerer measured the mean and fluctuating axial velocities along the combustor centerline using Laser Doppler Velocimetry. He was able to deduce the local displacement turbulent flame speed by inferring the velocity of the flow entering the leading edge of the flame (or anchoring point) was equal to the local turbulent displacement flame speed $S_{t,LD}$.

A modification of equation 2.9 leads to

$$S_{t,LD} = S_l + Cu' \quad (2.10)$$

where C is an empirical constant, derived from experiments. If u' is significantly larger than S_l , equation 2.10 can be reduced to

$$S_{t,LD} = Cu' \quad (2.11)$$

D. Beerer measured u' and $S_{t,LD}$ in his experiment runs and determined C as approximately 2.1 for lean premixed methane flames.

3 Simulations

3.1 Domain and mesh

The experiment, described in chapter 2, is modeled as a 2-dimensional, axisymmetric setup, due to limited computational resources. Steady state, Reynolds-Averaged-Navier-Stokes (RANS) simulations are conducted using the Software ANSYS Fluent, version 14.0. A structured, quadrilateral mesh, with 1 mm cell length in both spatial directions is employed as a base mesh. It consists of 31 000 cells. A picture of the mesh can be found in the Appendix A.5. A mesh refinement analysis can be found in Section 4.2.2. The domain is shown in figure 3.1. Additionally, a drawing of the domain with all dimensions can be found in the Appendix A.6.

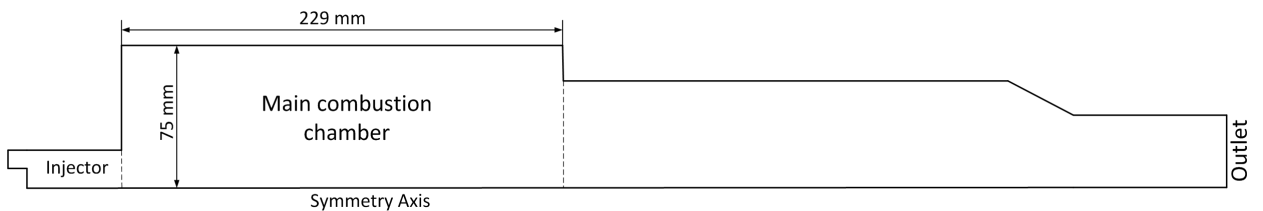


Figure 3.1: Domain for simulations

3.2 Boundary conditions

For modeling the Low Swirl Injector (LSI) two mass flow inlets are used. Mass flow inlets allow the user to specify the direction of the flow, which is not possible using pressure inlets. The perforated plate is modeled as the “center inlet”, with a velocity vector, consisting only of an axial component. The annulus, including the swirl vanes is modeled as the “swirl inlet”, using a velocity vector with an axial and a tangential component. Fluent allows the user to set up an axisymmetric simulation including azimuthal velocities (swirl). The injector, with the two mass flow inlets, and the sudden expansion nozzle are shown in figure 3.2. For better understanding of the dimensions in the combustion chamber, the location where the flame was anchored in the experiment (red dashed line) is added.

3.2 Boundary conditions

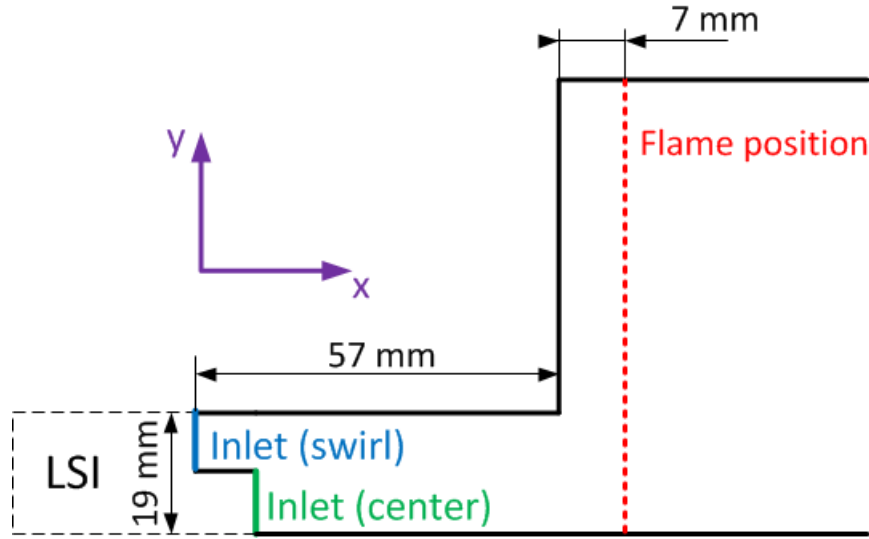


Figure 3.2: Detail of injector in domain.

In order to get a well-posed simulation setup, the exhaust outlet in the experiment setup is modeled with a pressure outlet condition. As the flow in the combustion chamber is viscous, all the walls are implemented as “nonslip walls”. The heat losses of the reactor are not known from the experiment. Therefore a calculation of the heat transfer coefficient is conducted, based on fully developed turbulent pipe flow. The result is a heat transfer coefficient of $h = 136.6 W/(m^2 K)$, which is specified for all walls in the domain, except for the sudden expansion wall. On that wall, the temperature is set to the temperature of the incoming fuel air mixture, i.e. 418K. Table 3.1 shows the most important parameters of the simulations. (The complete list of all parameters for the Cold Flow and Hot Flow simulations can be found in the Appendix, in Section A.3).

Parameter	Symbol	Value	Unit
Fuel	CH_4	100	%
Heat release of combustion	\dot{Q}	387	kW
Operating pressure	p_{op}	416136	Pa
Equivalence ratio	Φ	0.71	-
Inlet temperature of fuel-air mixture	T_{in}	418	K
Adiabatic flame temperature	T_{ad}	1950	K
Total mass flow rate	\dot{m}_{tot}	0.194	kg/s
Diameter of injector	d_{in}	38	mm
Average velocity in injector	U_0	49.4	m/s

Table 3.1: Parameters for simulations

One of the most challenging tasks during the simulations is to model the Low Swirl Injector (LSI). It is not possible to model 3-dimensional objects like swirl vanes or a perforated plate

3.2 Boundary conditions

in a 2-dimensional domain. Instead, it is decided to model the LSI with two mass flow inlets see figure 3.2. The total mass flow rate of the fuel-air mixture in the experiments is known, but not how the mass flow divides going through the LSI, an important piece of information for the simulation setup.

Based on Bernoulli's energy conservation equation for streamlines in incompressible flows, a mass flow split for the cold flow simulations is conducted. The mass flow through a nozzle is given by

$$\dot{m} = A_{eff} \sqrt{2\rho\Delta p_{LSI}} \quad (3.1)$$

where ρ is the density of air and $\Delta p_{LSI} = 13.1 \text{ kPa}$ the pressure loss over the Low Swirl Injector, measured in the experiment for cold flow at 4 atmospheric pressures. The effective area is calculated as

$$A_{eff} = C_{loss} A_{geo} \quad (3.2)$$

where A_{geo} is the geometric area. The Bernoulli approach calculation is an estimate to determine an initial value for the simulations. Therefore the loss coefficient C_{loss} is set to unity for both inlets.

$$\dot{m} = A_{geo} \sqrt{2\rho\Delta p_{LSI}} \quad (3.3)$$

For the center inlet, the geometric area is determined as the number of holes N_{holes} multiplied with the area of one hole A_{hole} .

$$A_c = N_{holes} A_{hole} \quad (3.4)$$

For the swirl inlet, the geometric area is calculated as the area of the annulus A_{ann} minus the area, blocked by the thickness of the swirl vanes, i.e. number of vanes N_{vanes} multiplied with the cross-sectional area of one vane A_{vane} .

$$A_s = A_{ann} - N_{vanes} A_{vane} \quad (3.5)$$

The calculated mass flow through the center inlet is

$$\dot{m}_c = A_c \sqrt{2\rho\Delta p_{LSI}} = 0.0379 \text{ kg/s} \quad (3.6)$$

and through the swirl inlet

$$\dot{m}_s = A_s \sqrt{2\rho\Delta p_{LSI}} = 0.1135 \text{ kg/s} \quad (3.7)$$

The total mass flow rate according to the Bernoulli approach calculation is 0.152 kg/s for cold flow, which is smaller than the total mass flow rate of 0.172 kg/s , measured with a mass flow meter during the experiment. The fraction of the total mass flow rate going through the center inlet is

$$F_c = \frac{\dot{m}_c}{\dot{m}_c + \dot{m}_s} = 0.25 \quad (3.8)$$

3.3 Settings in Fluent

and through the swirl inlet

$$F_s = \frac{\dot{m}_s}{\dot{m}_c + \dot{m}_s} = 0.75 \quad (3.9)$$

During the cold flow simulations, this mass flow split and two others, are simulated in order to verify the calculation results. The mass flow split that matches the measured axial velocity profiles from the experiments the best is 1 : 3.5 (Center : Swirl). This is discussed in more detail in chapter 4.1 (Cold flow simulation results).

The outlet angle of the swirl vanes in the LSI is $\alpha_{vanes} = 37^\circ$ to the axial direction. In reality the flow might not follow the swirl vanes exactly, so a reduced swirl angle $\alpha_{flow} = 35^\circ$ is found to be the best match with the measured axial velocity profiles, according to different cold flow simulation results, see chapter 4.1. To set the turbulence parameters of the flow at the mass flow inlets, it is chosen to specify a turbulent length scale l_t and a turbulent intensity, which is defined as u'/U_0 . For the center inlet, l_t is specified as the diameter of the holes in the perforated plate. For the swirl inlet, l_t equals the gap height of the annulus. The value for the turbulent intensity was based on the average value of u'/U_0 close to the sudden expansion, measured from centerline to the combustion chamber wall, during the corresponding experiment. Table 3.2 shows the specified parameters at the two inlets for the hot flow simulations.

Parameter	Symbol	Unit	Center Inlet	Swirl Inlet
Radius	r	mm	12	19
Mass flow split		%	22.5	77.5
Mass flow rate	\dot{m}	g/s	43.6	150.3
Swirl angle of flow	α_{flow}	°	0	35
Axial velocity component	U	m/s	27.8	63.6
Radial velocity component	V	m/s	0	0
Tangential velocity component	W	m/s	0	44.6
Turbulent Length Scale	l_t	mm	2.6	7
Turbulent Intensity	u'/U_0	%	26	26

Table 3.2: Parameters at the two mass flow inlets for hot flow simulations

3.3 Settings in Fluent

Pressure based, 2-dimensional, axisymmetric simulations including swirl are conducted. To calculate the density of air, the incompressible ideal gas model is chosen, as the Mach-numbers at the Inlets are smaller than 0.2. The 2-equation turbulence models, like the k- ϵ - model, assume that turbulence is isotrop. Those models normally do not bring good results for strongly rotating flows and flows with high streamline curvature, which is the case for the Low Swirl Burner. A more sophisticated way of modeling turbulence is the Reynolds-Stress-Model, which considers the anisotropy of the Reynolds Stress Tensor. One equation for each component

3.4 Combustion models

of the Reynolds Stress Tensor is solved [2]. For the viscosity model in Fluent, the Reynolds-Stress-Model with “linear pressure strain” is used. As the mesh is not fine enough to resolve the boundary layers on the walls, the “enhanced wall treatment” is chosen. This option combines the two-layer model with enhanced wall functions. Where the mesh is fine enough, the two-layer model is used. In the regions with a coarse mesh, the enhanced wall functions, which are a set of semi-empirical functions, are used to bridge the viscosity affected region between the wall and the fully turbulent flow. In the two-layer model, the complete domain is divided into a viscosity affected region and a fully turbulent region [8].

To solve the combustion chemistry, the Eddy Dissipation Concept model and the Turbulent Flame Speed Closure model (“Premixed-model” in Fluent) are used in separate simulation runs. These models will be described more in detail in the next Section 3.4. For the pressure velocity coupling the SIMPLE solver is used. In order to achieve good stability, the first simulation runs are executed with First Order Spatial Discretization methods for all variables. When a converged solution is achieved, the Spatial Discretization method is changed to Second Order for all variables. For the pressure solver, the PRESTO method is chosen, because the Fluent User’s Guide [9] suggests this method for strongly swirling flows.

3.4 Combustion models

3.4.1 Eddy Dissipation Concept model

The equations in this chapter and the explanations can be found in the Fluent Theory Guide [8]. This model, which is an extension of the Eddy Dissipation model, allows the inclusion of detailed chemical mechanisms in turbulent flows. It assumes that turbulent mixing rates control the combustion, which means high Da-numbers. This model is based on the energy cascade of the turbulent energy. It assumes that the combustion reactions occur in the small turbulent structures, called the fine scales (* marks the fine scale quantities), where the energy is dissipated. Considering one cell, the fine scales take up a certain fraction of it, which can be expressed as the volume fraction of the fine scales

$$(\xi^*)^3 = C_\xi^3 \left(\frac{\nu \epsilon}{k^2} \right)^{3/4} \quad (3.10)$$

ξ^* is the length fraction of the fine scales, C_ξ the volume fraction constant, ν the kinematic viscosity, ϵ the turbulent eddy dissipation and k the turbulent kinetic energy. In a cell, the species are assumed to react in a perfectly stirred reactor with the current species and temperature of the cell at initial conditions. Additionally, it is assumed that the species react in the fine structures over a time scale

$$\tau^* = C_\tau \left(\frac{\nu}{\epsilon} \right)^{1/2} \quad (3.11)$$

where C_τ is the time scale constant.

The mean reaction rate of a computational cell is then modeled as a mass transfer between the fine structure regions in the cell and the rest of the fluid in the same cell. In the conservation equation of the mean species i , the source term is modeled as

$$\mathcal{R}_i = \frac{\rho(\xi^*)^2}{\tau^*[1 - (\xi^*)^3]}(Y_i^* - Y_i) \quad (3.12)$$

Y_i is the average mass fraction of species i and Y_i^* is the fine scale species mass fraction after reacting over the time τ^* . Having a closer look at equations 3.10 and 3.12, it can be seen that in areas of the flow where the values for the turbulent eddy dissipation ϵ are large, the reaction rates are high.

3.4.2 Turbulent Flame Speed Closure model

In this section, the Turbulent Flame Speed Closure (TFC) model, also called “Premixed model” in Fluent will be described. The information, including equations, can be found in the Fluent User’s Guide [9] and the Fluent Theory Guide [8]. This model is applicable for the “thin reaction zone” combustion regime, where the smallest turbulent scales in the flow are smaller than the flame thickness and are penetrating into the flame zone. This regime is characterized by Karlovitz-numbers greater than unity. For more information about the flame regime see Chapter 2.3. In contrast to the EDC model, this model does not include detailed reaction chemistry. Combustion is modeled through a reaction progress variable c , which is defined as sum of the product species, normalized with the sum of the product species at chemical equilibrium. That means, $c = 0$ represents the unburned and $c = 1$ the completely burned state of the fuel-air mixture. To model the flame front propagation, a transport equation for the reaction progress variable is solved.

$$\frac{\partial}{\partial t}(\rho \bar{c}) + \nabla \cdot (\rho \vec{v} \bar{c}) = \nabla \cdot \left(\frac{\mu}{Sc_t} \nabla \bar{c} \right) + \rho \mathcal{R} \quad (3.13)$$

This transport equation for c describes the spatial and temporal evolution of the reaction progress in a turbulent flow field. c is the mean reaction progress variable, Sc_t the turbulent Schmidt-number, \vec{v} the overall velocity vector, and μ the dynamic viscosity. The mean reaction rate \mathcal{R} in the source term is modeled as

$$\mathcal{R} = \rho_u S_t |\nabla c| \quad (3.14)$$

where ρ_u is the density of the unburned mixture and S_t the turbulent flame speed. In order to close the problem, the Zimont model for S_t is used, which is based on the assumption of equilibrium small scale turbulence in the laminar flame. For that reason, the turbulent flame speed is only dependent on large scale turbulence parameters.

$$S_t = C_z (u')^{3/4} S_l^{1/2} \alpha^{-1/4} l_t^{1/4} \quad (3.15)$$

C_z is a model constant, u' the velocity fluctuation, S_l the laminar flame speed, α the thermal diffusivity and l_t the turbulent length scale. A laminar flame speed $S_l = 0.23 \text{ m/s}$, calculated with CHEMKIN in D. Beerer’s PhD thesis [3], is specified as constant value in Fluent.

3.5 Stability and convergence of the simulation runs

For performing simulations on combustion, it is important to run “cold flow” or “non reacting” simulations first. There are multiple reasons for this. Analyzing cold flow results, the simulation setup parameters can be modified in order to get better simulation results. Cold flow simulations need a lot less computational resources, in comparison to “reacting simulations”, which include chemistry. Additionally, non reacting simulations converge more easily. Also, a cold flow solution can be used as an initial solution for the reacting simulations. A “step by step approach” for the simulations is used and shown to avoid diverging simulations. That means, starting out with a simple and robust turbulence model, e.g. $k - \epsilon$ turbulence model and first order discretization methods. If a converged solution is achieved, then change to a more sophisticated turbulence model, in this case the Reynolds-Stress-Model. Once again, after a converged solution, change the discretization methods to second order, and so on.

Judging if a solution is converged can be rather challenging. The normalized residuals of the important simulation parameters (energy, continuity, velocities, k , ϵ ,...) are monitored during all calculations. For a solution to be converged, the normalized residuals have to be smaller than $1 \cdot 10^{-6}$ and flat for a few thousand iterations. Another way of judging convergence is the “Report” function in Fluent, with which the overall mass- and energy-balance is checked. The error of the mass-balance in the cold flow simulations is smaller than $1 \cdot 10^{-6}$. In the hot flow simulations, the error of the mass-balance is smaller than $1 \cdot 10^{-9}$. The error of the energy-balance is smaller than $60W$, which means smaller than 0.016%, considering a total heat release of $387kW$ during combustion.

4 Simulation results

4.1 Cold flow

From the cold flow experiment runs, axial velocity profiles in the radial direction are available. Those profiles were measured a few millimeters downstream of the sudden expansion nozzle. (The location where the flame is anchored in the reacting experiment runs is 7mm , see Figure 3.2.) From centerline outwards, the velocity was measured in 1mm increments. As the Low Swirl Injector is modeled with two separate inlets in the simulations, the center inlet, representing the perforated plate and the swirl inlet, representing the annulus, different parameters have to be specified at those inlets. Sets of cold flow simulations are undertaken, to find out which settings match the experimental data the best, and are then used for the reacting simulations.

The first set of simulations is performed at 1 atmospheric pressure, in order to determine the velocity components at the two mass flow inlets. The center inlet only has a normal velocity component, whereas the swirl inlet has a normal and a tangential component. It is not clear if the flow perfectly follows the vanes in the annulus, meaning the flow angle being the same as the vane angle. In most applications the actual angle of the flow is smaller than the angle of the vanes. For that reason, three simulations with different flow angles are conducted. One with the flow angle equal to the vane angle of 37° , one with a reduced flow angle of 35° , and one with a further reduced flow angle of 30° . Those angles are in relation to the normal direction of the flow. A smaller flow angle means the tangential velocity component is smaller. The mass flow split for this series of simulations is 1 : 3 (Center : Annulus) Looking at the results of those three simulations in Figure 4.1, the one with the flow angle of 35° shows the best match with the measured axial velocity profiles in radial direction.

4.1 Cold flow

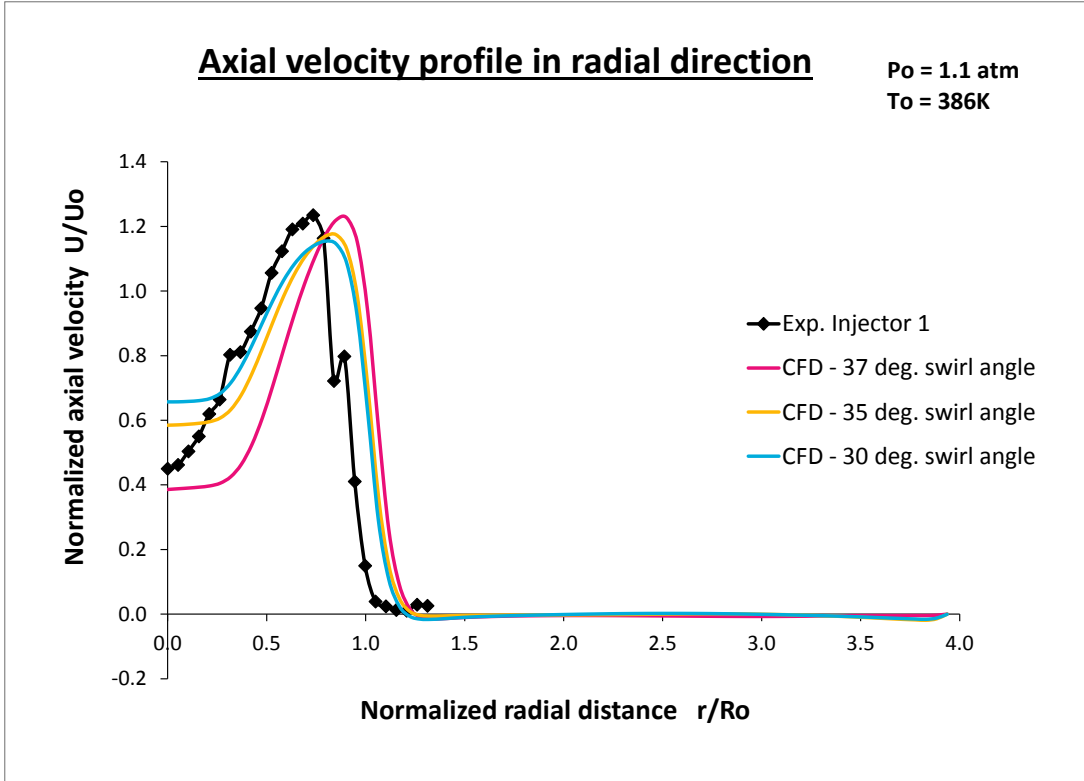


Figure 4.1: Operating pressure = 1 atm. Axial velocity profile in radial direction. Measured at 6mm downstream of the sudden expansion nozzle. Mass flow split 1 : 3 (Center : Annulus). Comparison of experimental data (with Injector 1) and simulation results with different swirl angles of the flow. Injector radius $R_0 = 19\text{mm}$, average velocity in injector $U_0 = 47\text{m/s}$.

Another important parameter is the mass flow split between the center inlet and the swirl inlet. The calculated mass flow split is 1:3 (Center : Annulus), so 25% through the center and 75% through the swirl annulus. In order to verify that split, three simulations with different mass flow splits are carried out and analyzed. This set of simulations is run at an operating pressure of $p_{op} = 4\text{atm.}$, at which the experiment with methane was conducted. The results are shown in figure 4.2. $R_0 = 19\text{mm}$ is the inner diameter of the inlet nozzle and $U_0 = 47\text{m/s}$ the bulk velocity in the inlet nozzle, calculated with the continuity equation.

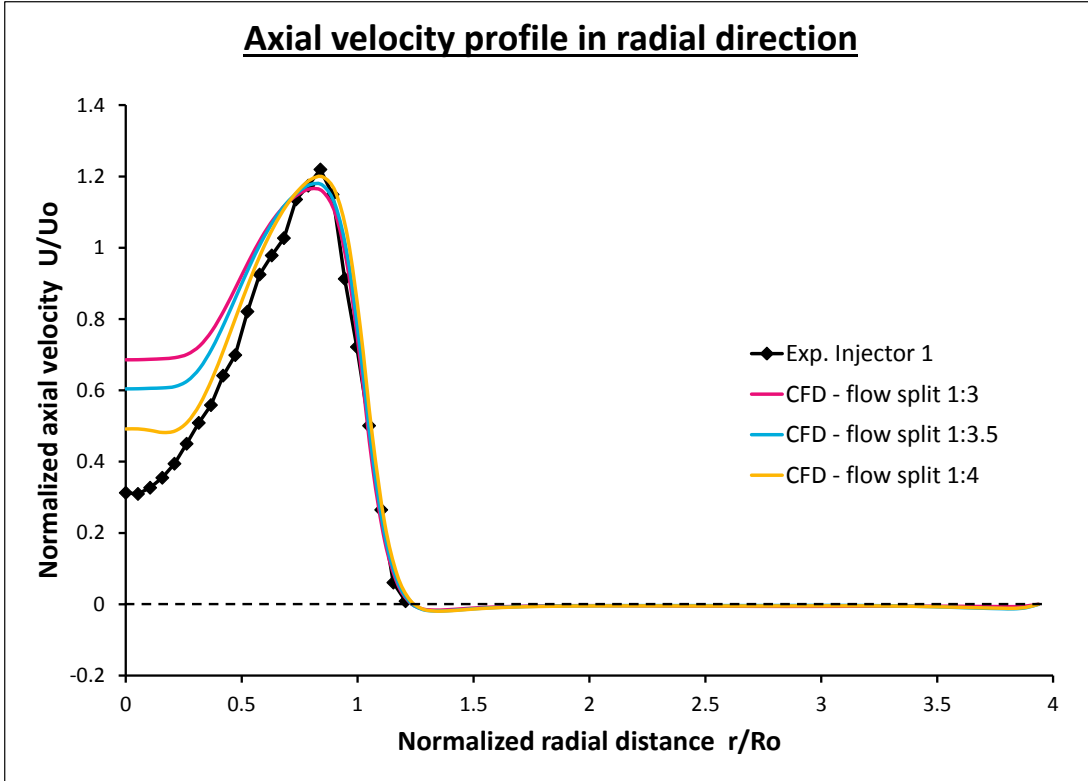


Figure 4.2: Operating pressure = 4 atm. Axial velocity profile in radial direction. Measured at 8mm downstream of the sudden expansion nozzle. Swirl angle = 35° . Comparison of experimental data (with Injector 1) and simulation results with different mass flow splits through the two inlets (Center : Annulus). $R_0 = 19\text{mm}$ and $U_0 = 47\text{m/s}$

The simulation results of the axial velocity profiles, of all mass flow splits, match well in the region of the swirl inlet (normalized axial distance 0.6 - 1). But the axial velocity profiles are all higher than the values from the experimental data in the region of the center inlet (normalized axial distance 0 - 0.6).

In order to make a decision on the mass flow split, the measured axial velocities on centerline from the experiments are also considered. Two different Low Swirl Injectors were used in the non reacting experiment runs. Injector 2 has slightly thinner swirl vanes and a smaller blockage ratio in the perforated plate than Injector 1, the other geometric features are the same. The results can be found in figure 4.3. The measured data with Injector 1 is inconsistent with the physical phenomenon of flow divergence and the thereby resulting axial velocity decay, as described in chapter 2.2. Together with the conductor of the experiments, D. Beerer, it was decided that for comparison of the centerline velocities, Injector 2 is the better choice. More details on the unusual behavior of Injector 1 can be found in D. Beerer's PhD thesis [3].

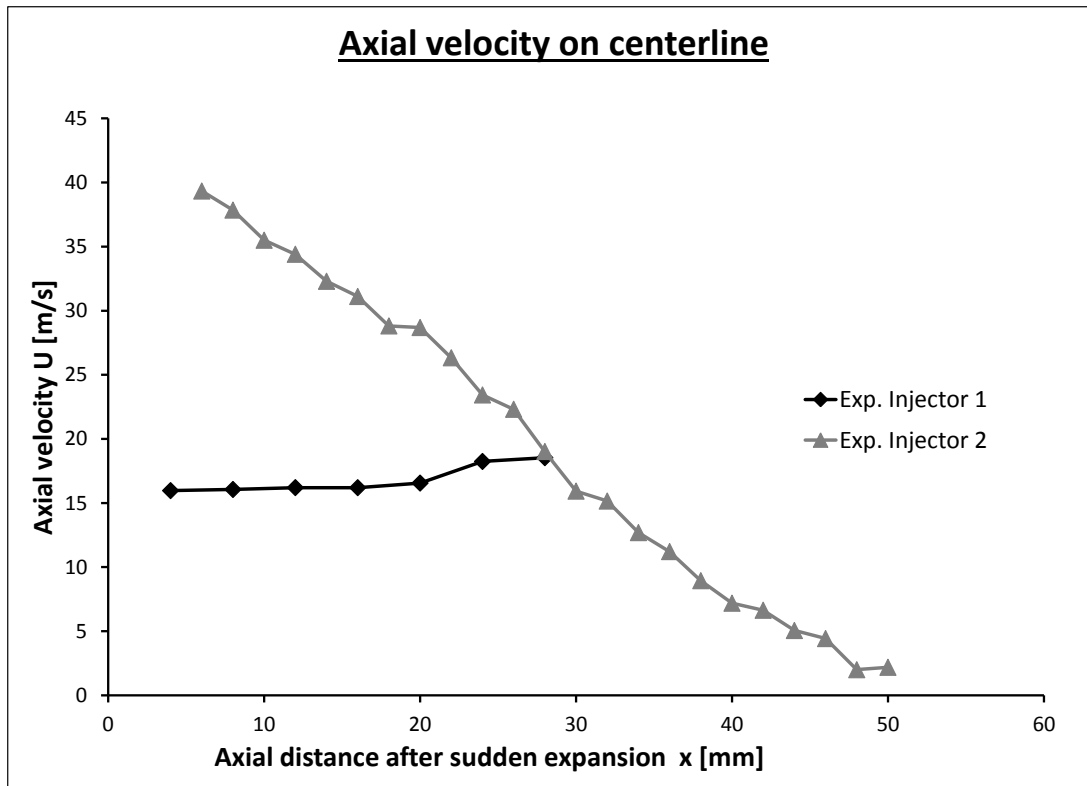


Figure 4.3: Axial velocity on centerline. Comparison of experimental data of two different Low Swirl Injectors.

Comparing the simulation results and the experimental data with Injector 2 in Figure 4.4, the mass flow split 1:3.5 is the best fit and is therefore used for the reacting simulations. For a different comparison, numerical integration of the axial velocity profiles in Figure 4.2 is undertaken, in order to determine the corresponding mass flow rates. The result shows that the calculated mass flow of the experimental data is 0.5% smaller than the calculated mass flow of the simulation result with the mass flow split 1 : 3.5. As the surface of the integral is proportional to the radius squared, the deviation of the axial velocity profiles on centerline does not result in a significantly different mass flow rate.

After the flow enters the combustion chamber, downstream of the sudden expansion, the flow diverges and the axial velocity decreases. In the reacting simulations, somewhere on the slope there is an equilibrium of the turbulent flame speed and the local axial velocity. That is where the flame is anchored. In the flow field of the simulations a central recirculation zone can be found, which can be seen in Figure 4.4 where the axial velocity is smaller than zero. This recirculation zone is not as strong as with High Swirl Injectors, but exists and increases the flow divergence in the combustion chamber.

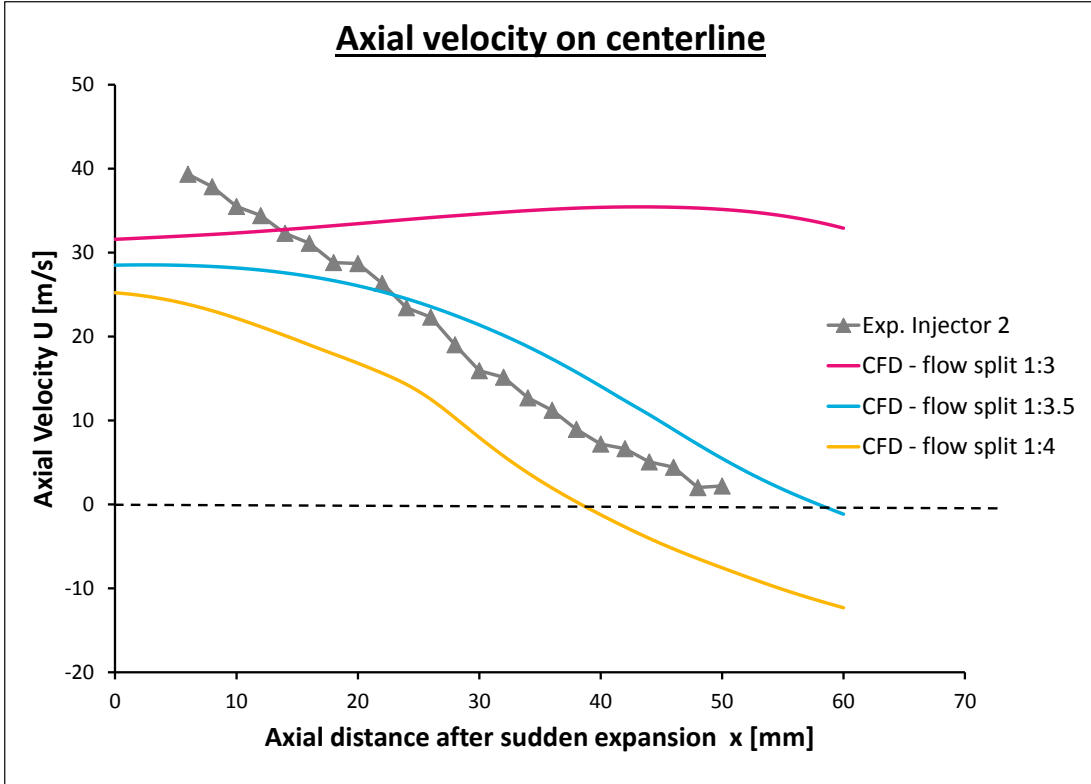


Figure 4.4: Axial velocity on centerline. Comparison of experimental data and simulation results with different mass flow splits through the two inlets (Center : Annulus).

Another important parameter, describing the flow field, is the Turbulence Intensity. It is defined as u'/U_0 in the experimental data, where u' is the measured turbulence fluctuation in axial direction and U_0 is the calculated average (bulk) velocity in the injector. The turbulent velocity fluctuation from the simulation results can be calculated from the Turbulent Kinetic Energy k . The following equation shows the relation between u' and k , for isotropic turbulence.

$$k = \frac{3}{2}(u')^2 \quad (4.1)$$

The calculated value for u' was then normalized with U_0 in order to compare the simulation results with the experimental data, see figure 4.5. The highest Turbulence Intensity in the radial profile can be seen in the region of the outer shear layer ($r/R_0 = 1$) in the experiment and in the simulation. A second, smaller maximum can be seen in the inner shear layer, between the two mass flow inlets ($r/R_0 = 0.6$). Qualitatively, both graphs show the same trend, but there is a quantitative difference on centerline and in the outer shear layer. The smaller

4.1 Cold flow

values on centerline are typical for 2-dimensional, axisymmetric simulations. The vortex core is not stable in reality, which results in higher values for the Turbulence Intensity.

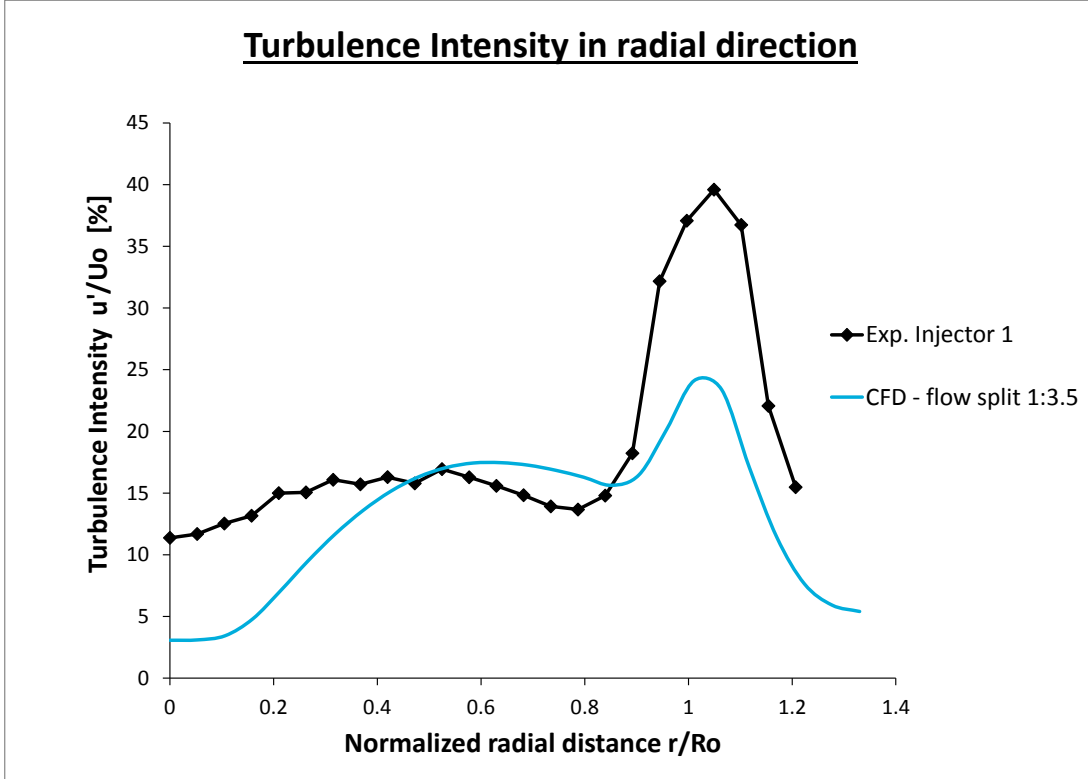


Figure 4.5: Turbulence Intensity from experiments and simulations. $U_0 = 47\text{m/s}$, $R_0 = 19\text{mm}$.

The findings of the cold flow simulations are the following. The best results can be achieved with a swirl angle of the flow $\alpha_{flow} = 35^\circ$ and a mass flow split of 1 : 3.5 (Center : Annulus). These settings are used for the reacting simulations, described in the next section 4.2. And this cold flow solution is also used as initial solution for the reacting flow simulations. An overview of the settings at the mass flow inlets can be found in Table 3.2.

4.2 Reacting flow

4.2.1 Plots of flame shape and position

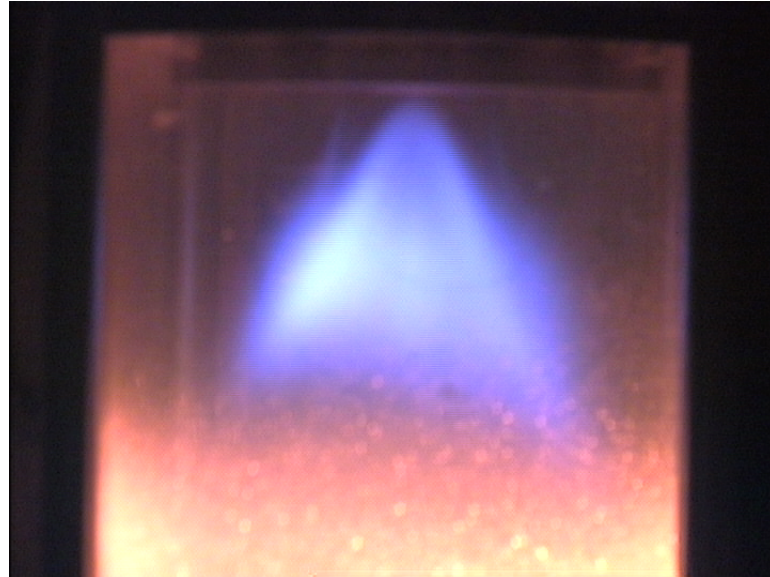


Figure 4.6: Photo of flame with pure methane as fuel, taken during the experiment.

In this section, the simulation results with the Eddy Dissipation Concept combustion model (EDC-model) and the Turbulent Flame Speed Closure combustion model (TFC-model), are compared with the photos of the flame, taken by D. Beerer, during the experiments. All the flame photos were provided by the courtesy of D. Beerer. Figure 4.6 shows the sudden expansion nozzle and the upper part of the combustion chamber (quartz tube). The blue line shows the excited CO_2 molecule, a reaction product. That means the flame zone, where the highest reaction rates occur, is right above the blue line and its shape resembles an upside-down "V".

The first combustion model that is applied in the reacting simulation, is the EDC-model. A "skeletal mechanism" including 22 species of the methane combustion, developed by M. Karalus at University of Washington, is used in Fluent. That combination was used for simulation of a backmixed Jet Stirred Reactor in the combustion research group at University of Washington and brought results that matched the corresponding experiment [10]. The flame in that Jet Stirred Reactor is stabilized by the outer recirculation zone, which brings hot reaction products to the incoming fuel-air mixture. That is different to the stabilization mechanism of the flame in the Low Swirl Burner, explained in Chapter 2.2. The advantage of the EDC-combustion-model is that it can model individual species, involved in the combustion process. For that reason, emissions analysis (specifically CO and NOx) can be done with this model, which is a particular interest in this research. The results are compared with a photo of the flame. In the simulation, the flame zone, which means the area with the highest chemical reaction rates, is expressed with the "destruction rate of methane". In Figure 4.7 one can see a plot of the destruction rate of methane on the right half and the photo of the flame on the left half. The color red indicates a high methane destruction rate.

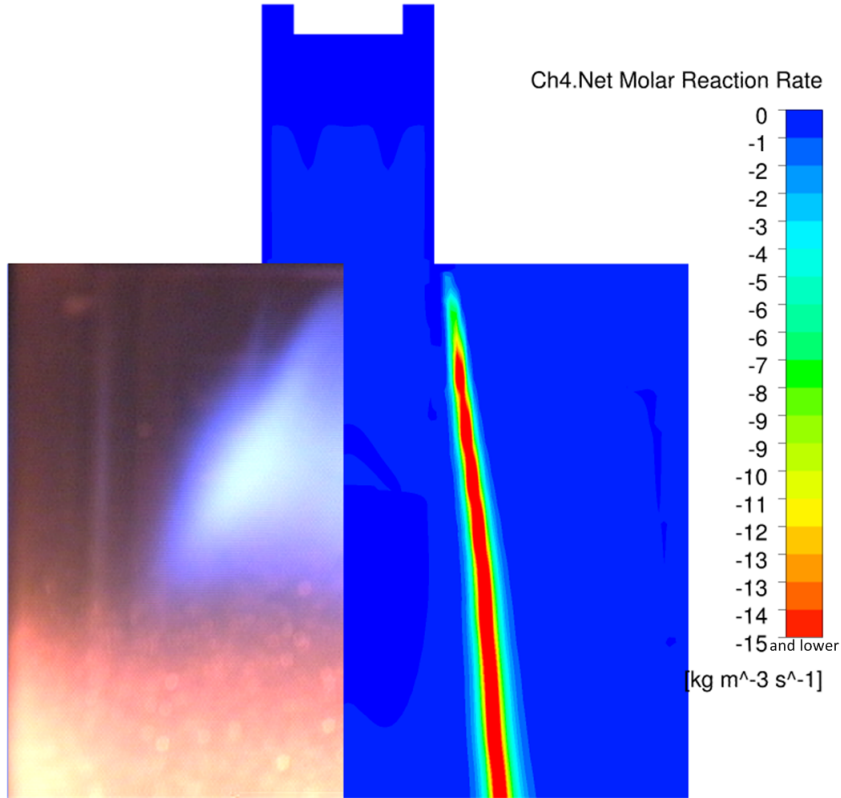


Figure 4.7: Comparison of flame shape and position of simulation with EDC-model (right) and flame photo from experiment (left). Variable indicating the flame in simulation with EDC-model: Destruction rate of methane. Red indicates rates of $-15 \text{ kg}/(\text{m}^3 \text{s})$ and lower.

The EDC-combustion-model predicts high reaction rates in the outer shear layer, where the incoming flow mixes with the fluid in the combustion chamber. The hot reaction gases in the outer recirculation zone ignite the incoming fuel-air mixture. In reality the high shear rates quench the flame in the outer shear layer. The EDC-combustion-model predicts high reaction rates in areas where the Turbulence Eddy Dissipation ϵ is high, which is the case for the outer shear layer. Diagram 4.8 shows that the destruction rate of methane is the highest where ϵ has its distinct maximum. This maximum occurs around the normalized radial distance of unity, which represents the location of the injector lip. The flame seems to be attached to the injector lip according to the simulation results. In contrast, the experimental results show that the flame is lifted, and stabilized by the equilibrium of the turbulent flame speed and the axial flow velocity on centerline. It seems that the EDC-model cannot model the upstream flame propagation on centerline correctly.

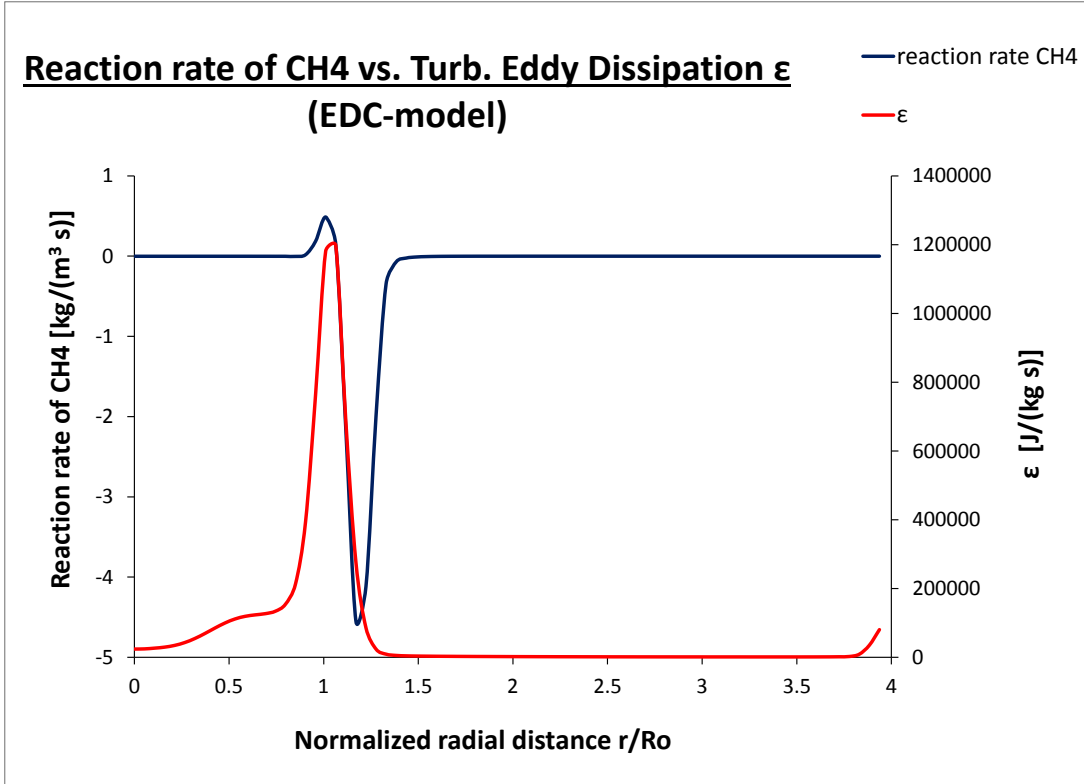


Figure 4.8: EDC-combustion-model. Radial profiles at 8mm downstream of the sudden expansion nozzle. Injector radius $R_0 = 19\text{mm}$.

In the TFC-combustion-model, the flame region is characterized by the product formation rate. Figure 4.9 shows the plot from the simulation on the right side. The color red indicates a high product formation rate, which is the equivalent to a high fuel destruction rate. The simulation result shows two locations of high product formation rates. Location one is on centerline in an upside-down V-shape, which can also be clearly seen in the photo of the flame in the experiment on the left side. (A complete plot of the product formation rate can be found in the Appendix A.2). Location two is in the outer shear layer. Looking closely at the flame photo, a flame strand can be seen in the outer shear layer as well, which means reaction is possible there. The flame in the experiment wants to stabilize in the outer shear layer, but gets pushed downstream by the incoming fuel-air mixture. Looking at the video of the flame, the outer flame strand fluctuates up- and downstream. In the experiment, the high shear rates quench the flame in the outer shear layer. The TFC-model does not account for the high strain rates extinguishing the flame in the outer shear layer. Research at the Technical University of Munich was done on improvement of the TFC-model in swirl-stabilized flames. L. Tay Wo Chong et al. found out that strain and heat losses have a strong effect on the laminar

4.2 Reacting flow

flame speeds [5]. Therefore the laminar flame speed was made a function of the local strain and heat losses, which made it possible to quench the flame in the outer shear layer in those simulations, where the corresponding experiment did not show reactions. In contrast, for the simulations in this research a constant laminar flame speed is specified.

During the experiment runs by D. Beerer, also blends of methane and hydrogen were used. Figure 4.10 shows the flame for a fuel mixture of 90% hydrogen and 10% methane. In that case, the flame is attached to the injector lip. As the turbulent flame speed of hydrogen is higher than the one of methane, the flame can propagate further upstream.

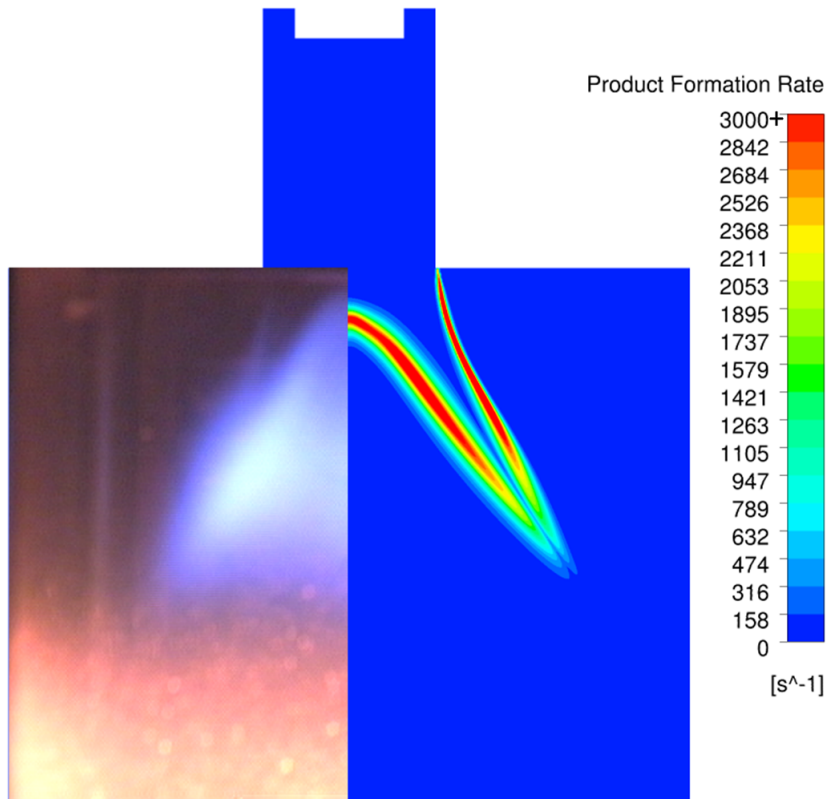


Figure 4.9: Comparison of flame shape and position of simulation with TFC-combustion-model (right) and flame photo from experiment (left). Variable indicating the flame in simulation with TFC-combustion-model: Product formation rate. Red indicates formation rates of 3000s^{-1} and higher.

4.2 Reacting flow

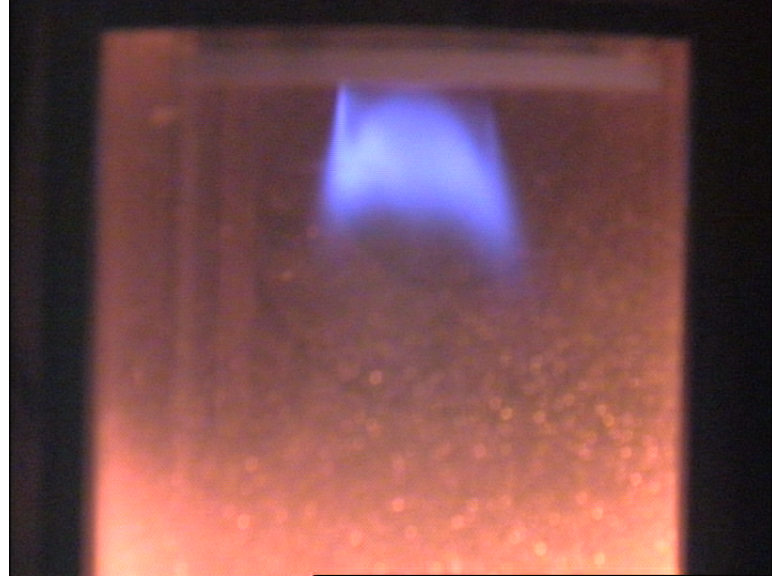


Figure 4.10: Photo of flame with a blend of 90% hydrogen and 10% methane as fuel, taken during the experiments.

The two combustion models predict the high reaction rates in different locations. Another significant difference is the modeled reaction progress in the combustion chamber. As it can be seen in the flame photos, the combustion reactions happen on centerline, very close to the sudden expansion nozzle in the experiment. In Figure 4.11 on the left side, the reaction progress in the simulation with the EDC-model is shown with the mass fraction of methane. For better comparison, the color legend is inverted, which means that blue represents the mass fraction of methane at the inlets and red a mass fraction of methane close to zero, at the end of the combustion process. On the right side, the reaction progress according to the TFC-combustion-model is shown with the reaction progress variable c . This qualitative comparison shows that the combustion reaction in the TFC-combustion-model simulation is happening very close to the injector nozzle, which matches the experiment. The TFC-model is able to predict the upstream flame propagation on centerline, by directly modeling the turbulent flame speed, as explained in Section 2.3 . In contrast, the EDC-combustion-model is not able to model the flame propagation on centerline correctly. A reason for that could be the insufficient modeling of the upstream diffusion of the combustion products.

4.2 Reacting flow

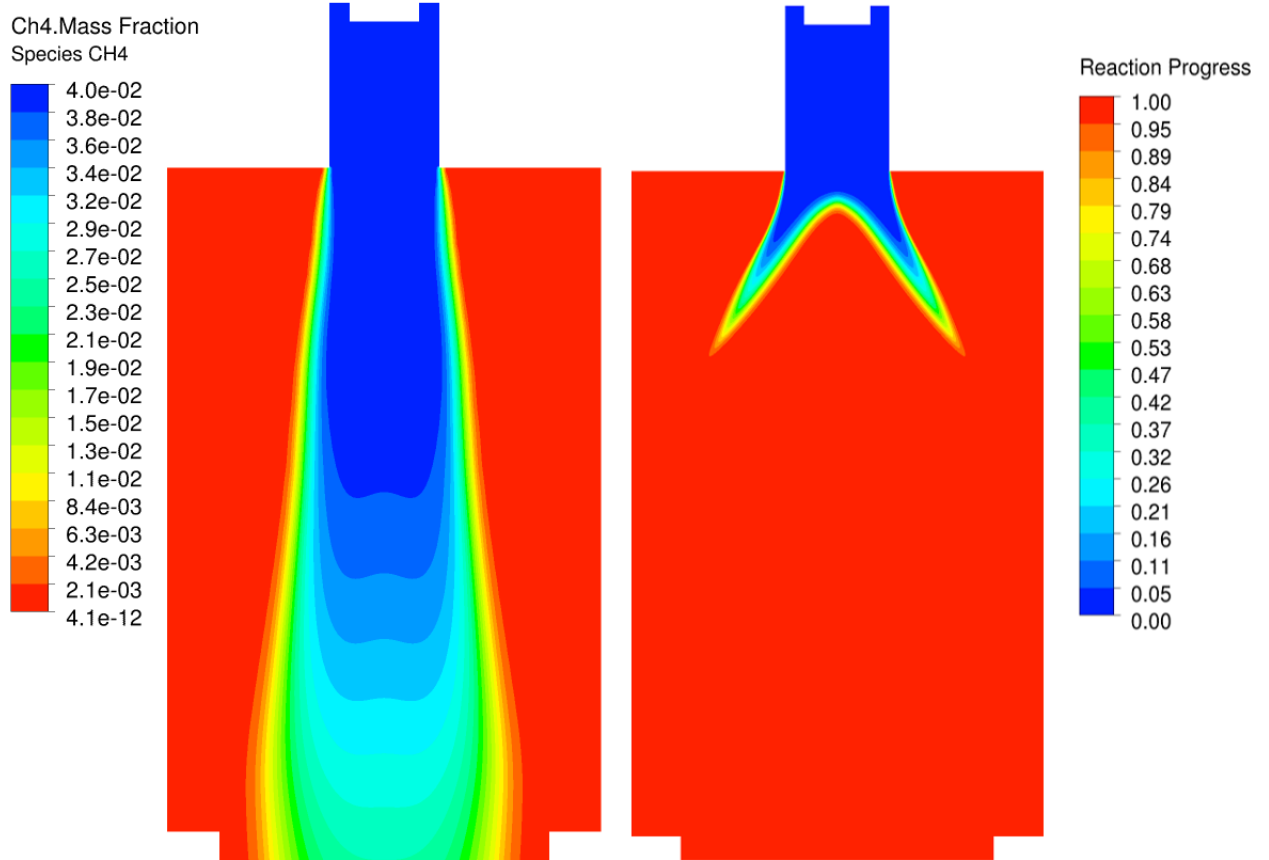


Figure 4.11: Qualitative comparison of the reaction progress in the two different simulation approaches. Left side: EDC-model. Right side: TFC-model. Note: The legends on the left and the right side are different.

A report, published by H. Pitsch at Stanford University [11], contains results of Large Eddy Simulation (LES) of a scale-up version of the Low Swirl Injector used in this research. The LES was conducted on lean premixed methane flames with an equivalence ratio of $\Phi = 0.59$ (For comparison: $\Phi = 0.71$ in this research). Figure 4.12 shows a qualitative comparison of the reaction progress and the flame shape in the RANS simulation of this research and the Large Eddy Simulation. On the left, the result of the TFC-combustion-model can be seen. On the right, an instantaneous temperature plot, representing the reaction progress for the LES, can be seen. The formation of detached combustion regions or isles and the strongly corrugated flame front can be seen in the plot. These characteristics are typical for the “flamelets in eddies” combustion regime, see Chapter 2.3. The plot on the right also shows the distinctive upside down V-shape of the flame on centerline, which can also be seen on the left side of Figure 4.12.

4.2 Reacting flow

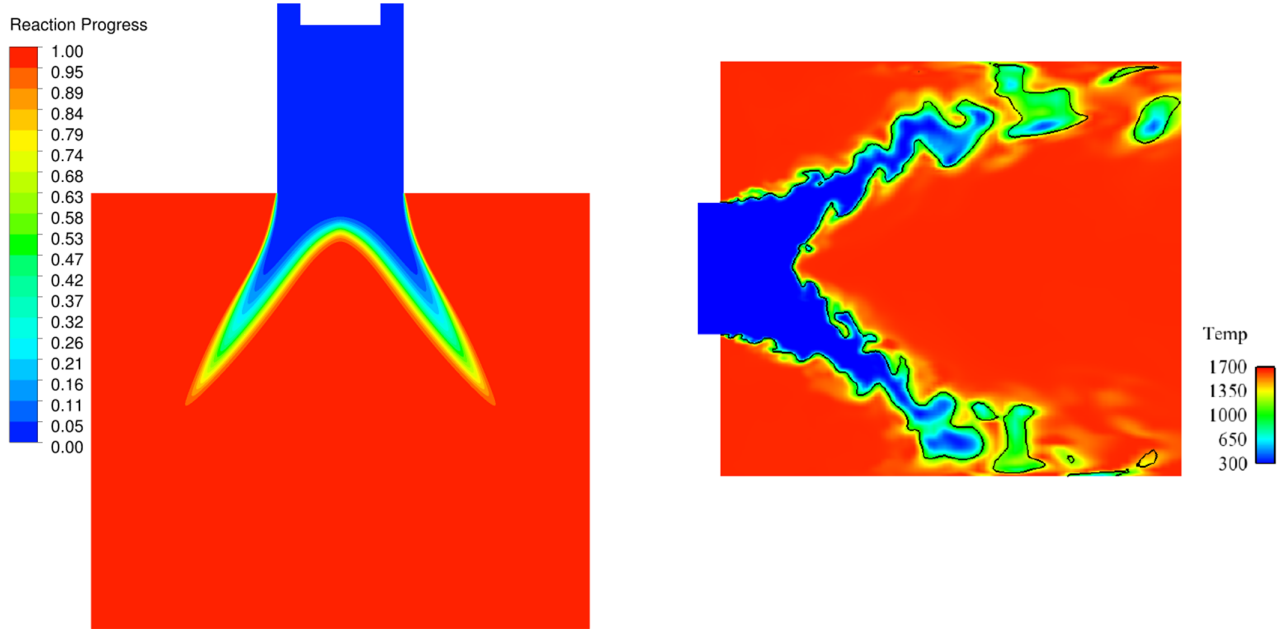


Figure 4.12: Qualitative comparison of reaction progress. Left side: Reaction progress variable c plot of result with TFC-model. Right side: Temperature plot of result with Large Eddy Simulation on a scale-up version of the Low Swirl Injector [11]

In Figure 4.13 on the left, the streamlines, colored by the local velocity, in the main combustion chamber can be seen. The right side shows the axial velocity plot. Both plots are extracted from the simulation with the TFC-combustion-model. The incoming flow diverges downstream of the sudden expansion nozzle, as explained in Chapter 2.2 and hits the inner combustion chamber wall around half way downstream of the main combustion chamber (quartz tube). The plot also shows the outer recirculation zones in the corners close to the sudden expansion nozzle and the central recirculation zone, which is larger and stronger. A plot of the radial velocity (Figure A.3) can be found in the Appendix.

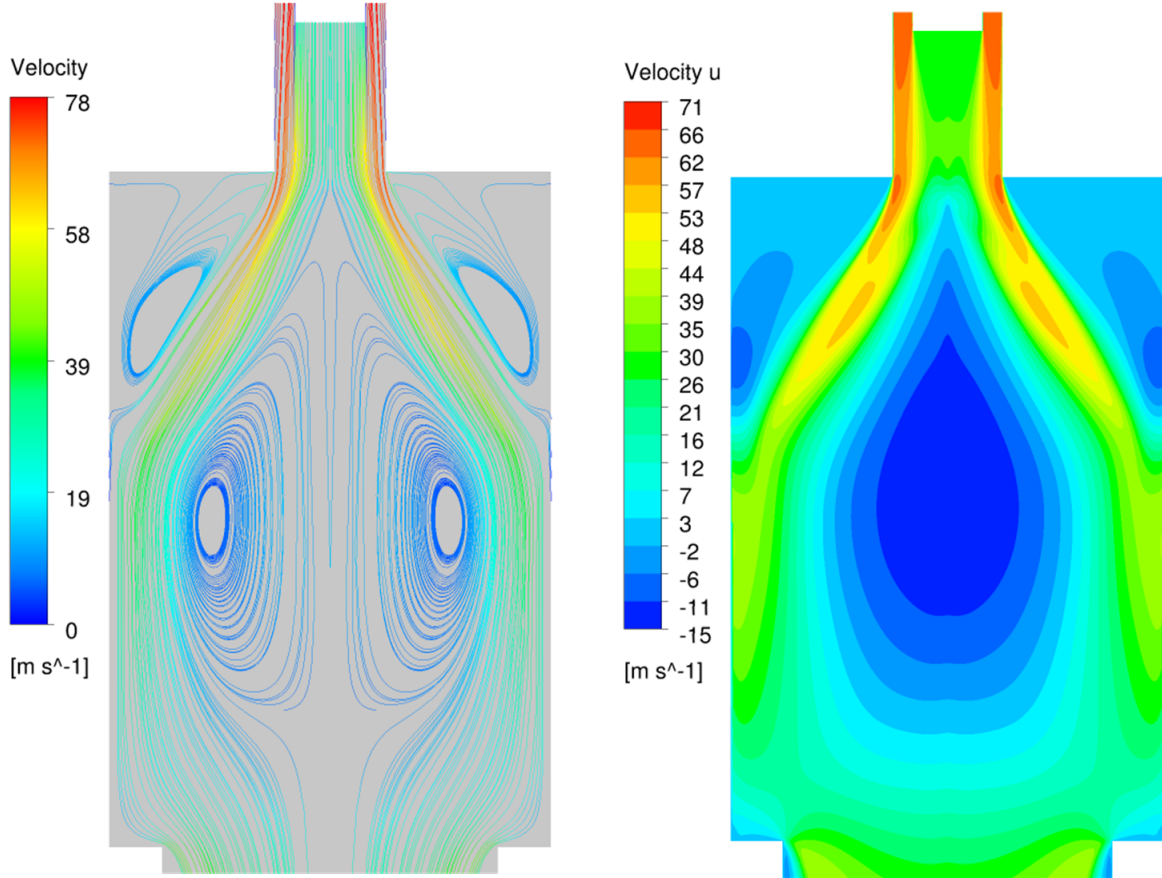


Figure 4.13: TFC-combustion-model. Left side: Streamlines, colored by the local velocity. Right side: Axial velocity plot.

In a publication by M. Day et al. [6] a normalized axial velocity plot can be found (Figure 4.14). The plot was made with measurements on a scale-up version of the Low Swirl Burner, at atmospheric pressure for an open (no enclosure) and up fired flame. The equivalence ratio of that lean premixed methane flame was $\Phi = 0.7$. The plot shows the existence of a central recirculation zone, marked with the dashed white line. As it was an open flame experiment, it does not have outer recirculation zones.

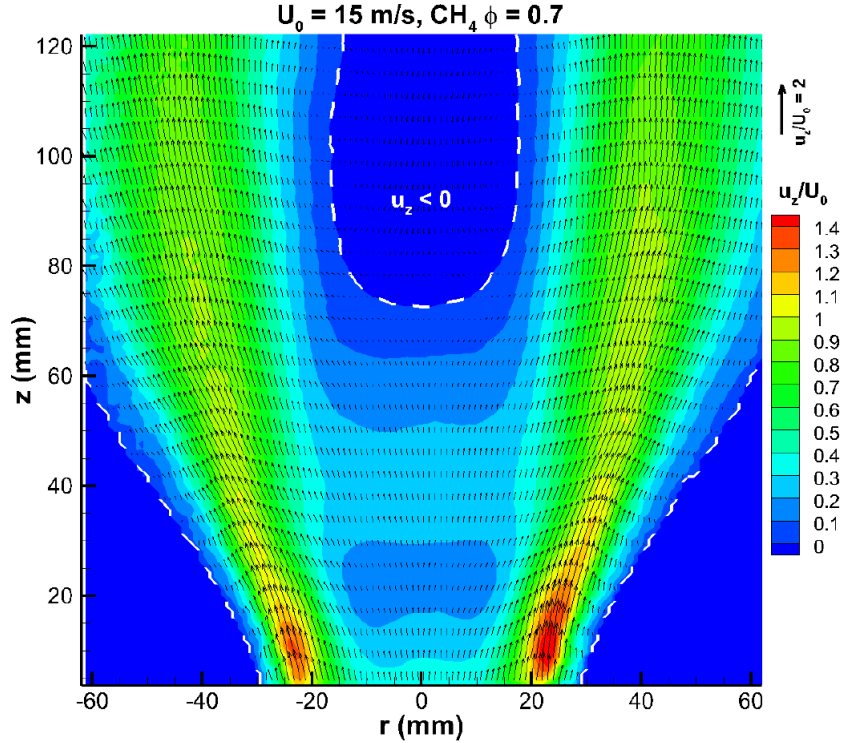


Figure 4.14: Velocity vectors and normalized axial velocity of scale-up Low Swirl Injector. Pre-mixed, open, up fired, methane flame at atmospheric pressure. [6]

4.2.2 Mesh independence study

After the first reacting simulation results are obtained, using the TFC-combustion-model and the standard mesh, a mesh independence study is carried out. Therefore, the base mesh is refined in the area of interest, which is the area with the high product formation rates (About the first third of the combustion chamber). For the first mesh refinement, the cell length in both spatial directions is halved to 0.5mm , which means each cell is divided in four equal cells. In order to check the result improvement, the product formation rate on centerline is used. The first mesh refinement increases the maximum value of the product formation rate and moves its location about 2mm closer to the injector. See Figure 4.15. Then, a second round of mesh refinement is undertaken, by repeating the first mesh refinement step in the area of interest, resulting in a cell length of 0.25mm . The second refinement, only moves the maximum value of the product formation rate a fraction of a millimeter closer to the injector, and it increases the maximum value slightly. With those results, it is decided that further mesh refinement would not bring better simulation results.

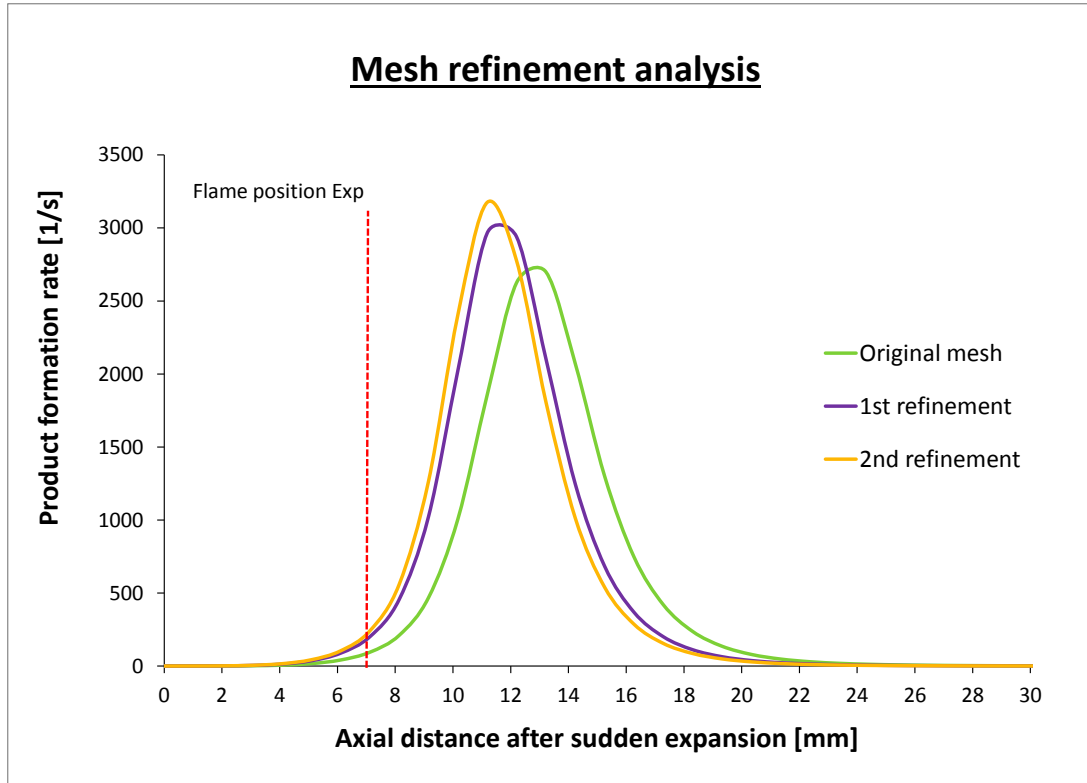


Figure 4.15: TFC-combustion-model: Results of mesh refinement in the first third of the combustion chamber

4.2.3 Diagrams

The flame anchoring point in the experiment was determined in different ways. One indicator was the axial velocity plot on centerline. Another indicator was the signal rate of the Laser Doppler Velocimetry measurements. The water droplets used for seeding evaporate when they reach the reaction zone, which reduces the signal rate.

The axial velocity on centerline, measured in the experiment, is compared with the simulation results of the TFC-combustion-model in Figure 4.16. For the reacting experiment run Injector 1 was used. The simulation result matches the experimental data well around the axial distance of 7 mm, which is where the flame anchoring point or leading edge of the flame is observed in the experiment. The axial velocity at that location is equal, but opposite to the turbulent displacement flame speed, which was measured to be $S_{t,LD} = 11.77 \text{ m/s}$ in the experiment. The axial velocity in the simulation with the TFC-combustion-model shows the linear decay that is expected due to the flow divergence, which is not consistent with the experimental data.

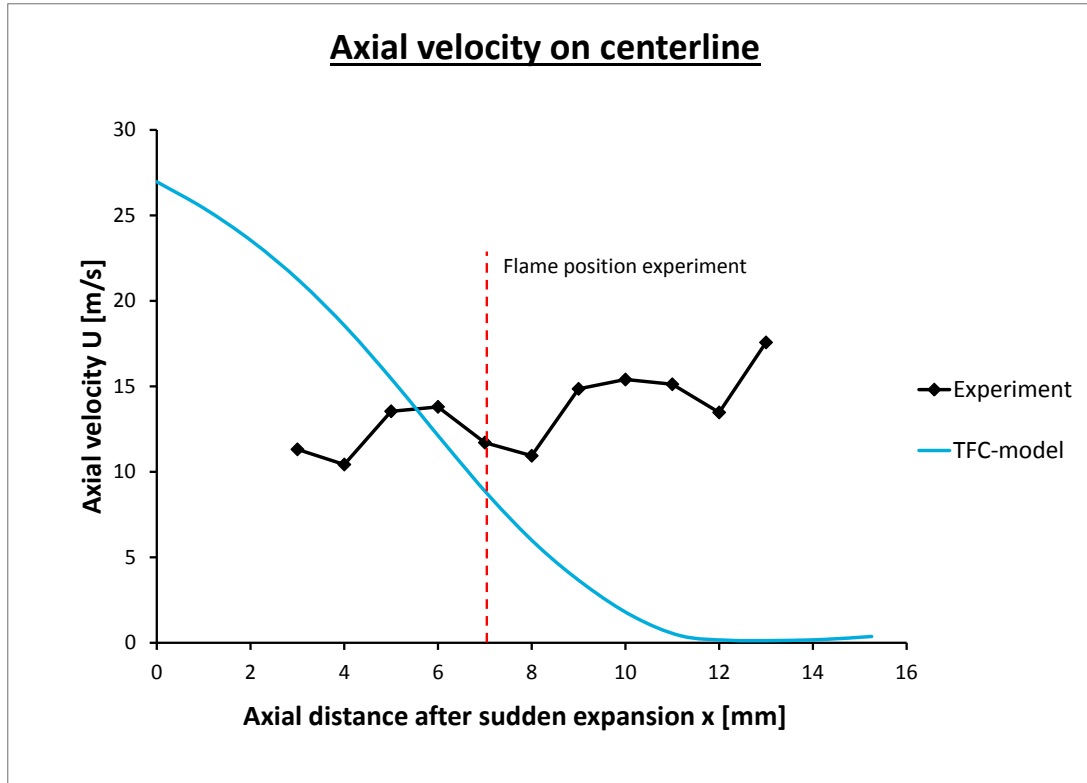


Figure 4.16: Axial velocity on centerline. Comparison of the results with the TFC-combustion-model and the experimental data (using Injector 1).

In the experiment, the axial velocity on centerline is an indicator for the local displacement turbulent flame speed. This is derived from the idea that the flame is anchored, where the turbulent flame speed is equal, but opposite to the local axial velocity of the incoming fuel-air mixture. The TFC-combustion-model correctly predicts this flame stabilization mechanism of the Low Swirl Injector. Figure 4.17 shows only results of the simulation with the TFC-combustion-model. The axial velocity (blue line) intersects with the modeled turbulent flame speed (green line) at the beginning of the flame zone, represented by the product formation rate (yellow line). The maximum of the product formation rate can be used as an indicator for the flame position in the simulation, which is around 11 mm downstream of the sudden expansion nozzle. The value for the modeled turbulent flame speed is approx. 4.5 m/s at that location. The axial velocity goes down close to zero in the post flame region and will become negative in the central recirculation zone further downstream. An additional diagram, including data further downstream (Figure A.1), can be found in the Appendix.

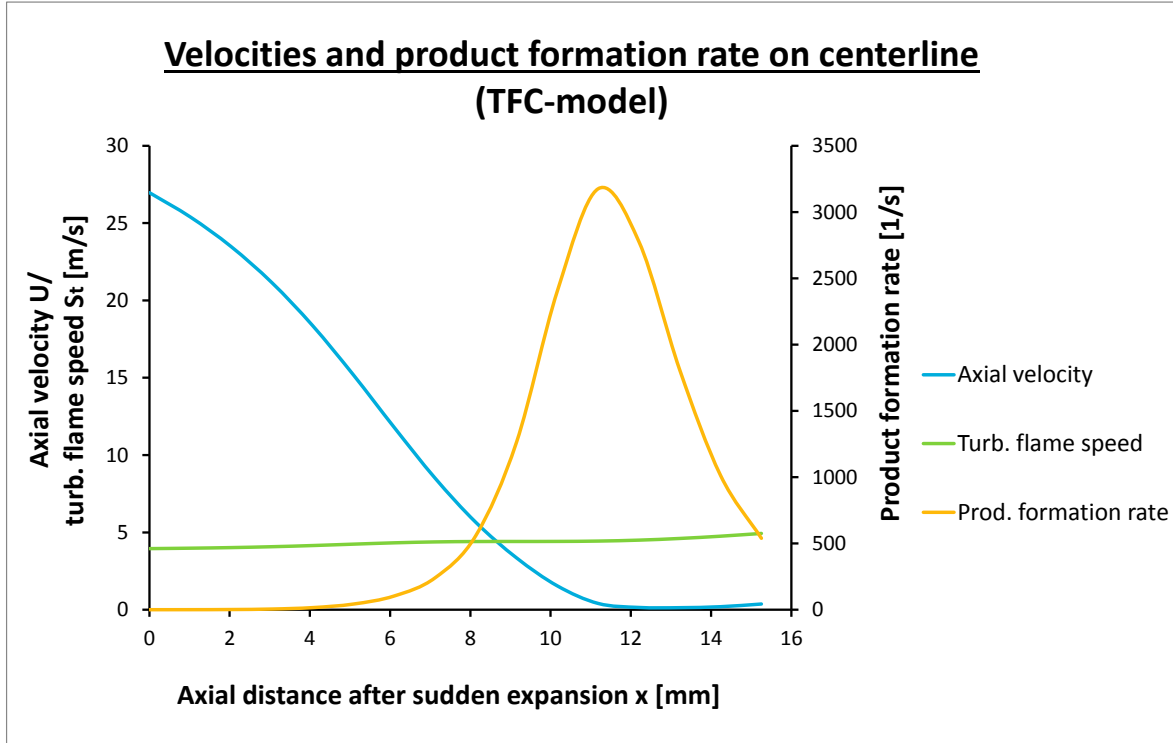


Figure 4.17: TFC-combustion-model: Parameters on centerline.

During the reacting experiment, the Turbulence Intensity was measured close to the sudden expansion nozzle on centerline. Figure 4.18 shows the experimental data, compared to the simulation result using the TFC-combustion-model. Both graphs show an increase of the Turbulence Intensity a few millimeters downstream of the respective flame zone. That means the combustion reactions, which increase the temperature and decrease the density of the fluid, induce additional turbulence in the flow.

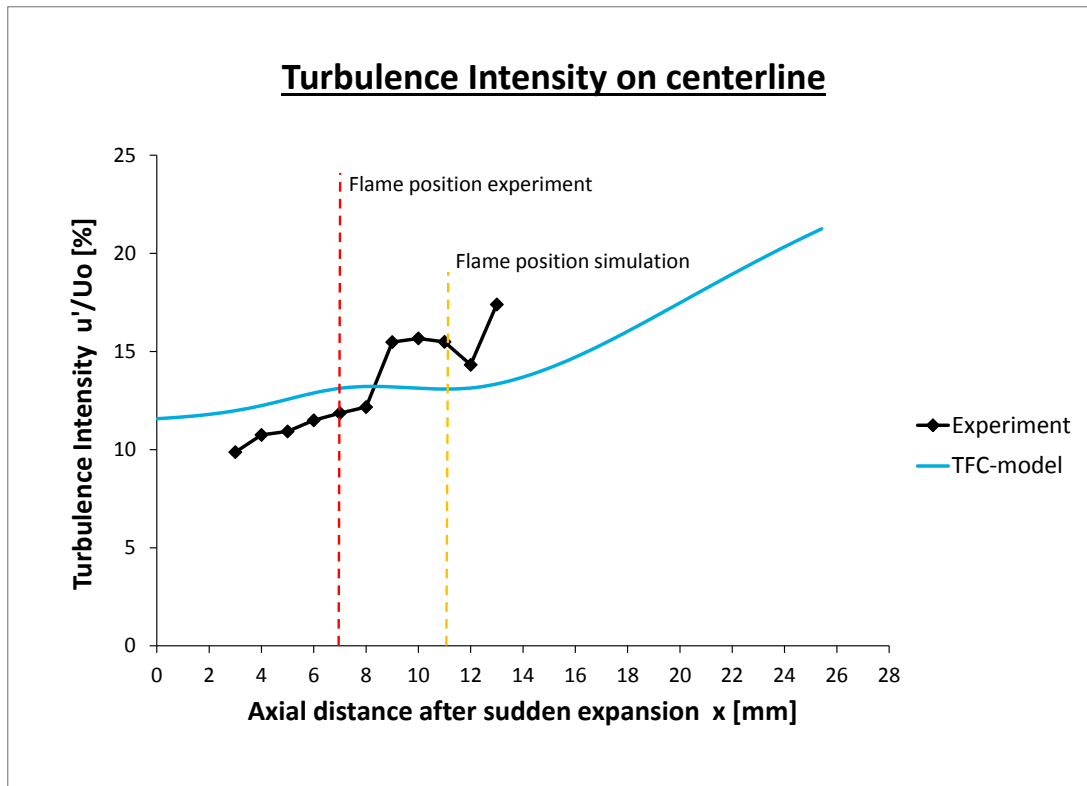


Figure 4.18: Comparison of Turbulence Intensity in simulation with the TFC-combustion-model and experiment (using Injector 1).

5 Conclusion

The intention of this research was to see, if the Low Swirl Burner can be modeled with a 2-dimensional, RANS simulation approach, using ANSYS Fluent 14.0. This approach is a major simplification of the reality. The first choice for the combustion model, was the Eddy Dissipation Concept model, because it can model individual species. Therefore, it can be used for emissions analysis. The original idea was to model the emissions from the Low Swirl Burner, and compare it with the experimental data. This research shows that the EDC-combustion-model is not able to predict the flame shape and position accurately, as it does not model the upstream flame propagation on centerline correctly. Thus, the result obtained from it cannot be used for emissions analysis in this particular case. This research suggests that the implementation of the EDC-combustion-model in simulation software should be improved, in order to use it for lifted low swirl flames. In a second approach, the Turbulent Flame Speed Closure model was used to simulate the combustion process. This model, which directly models the turbulent flame speed, predicts the flame shape and position correctly. However, it cannot account for individual species, involved in the combustion process. For the future, the results of this research could be used to do Chemical Reactor Network (CRN) analysis, to study the species involved in the Low Swirl Burner.

Another idea for future research would be to model the flow field of the Low Swirl Injector with non-reacting, 3-dimensional, Large Eddy Simulation, in order to get better values for the flow field, produced by the injector. Those results could then be used as input parameters for 2-dimensional, reacting, RANS simulation.

A Appendix

A.1 Additional diagrams

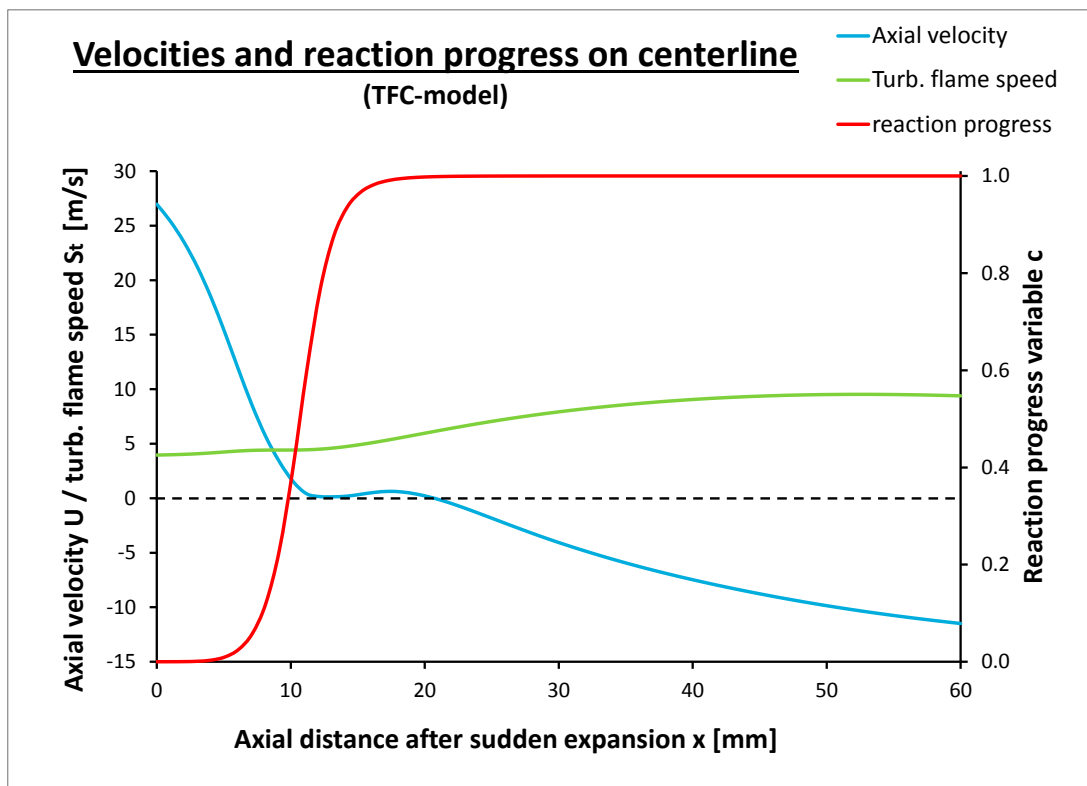


Figure A.1: Hot flow, at 4 atm. pressures. Parameters on centerline. Results of simulation with the TFC-model.

A.2 Additional plots

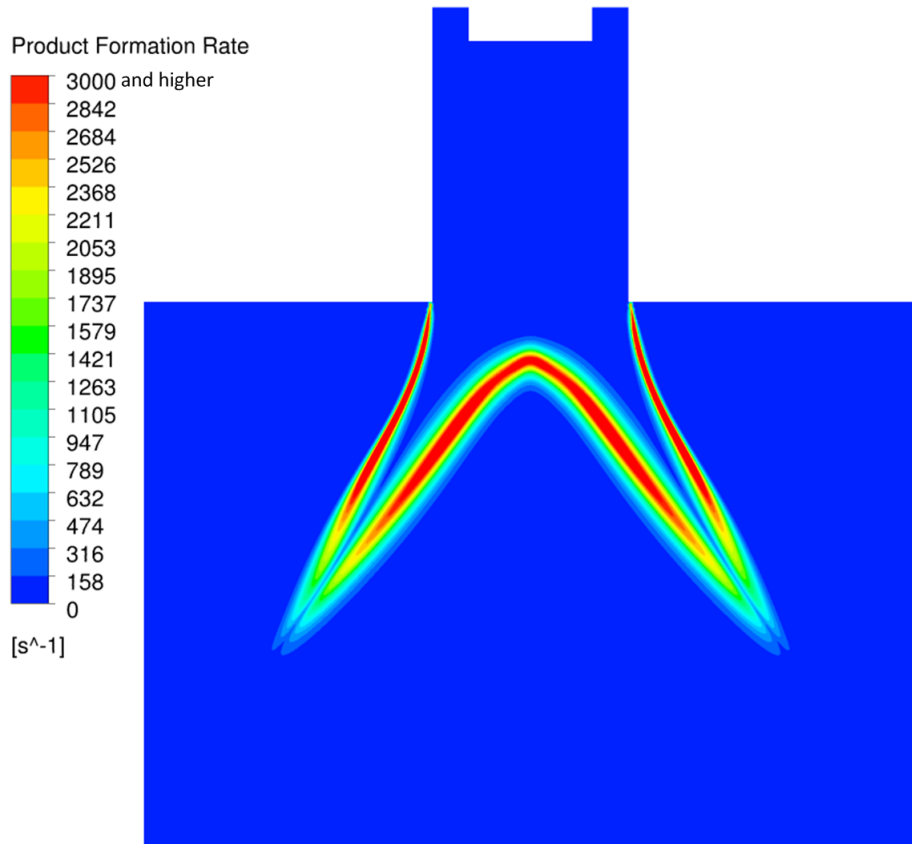


Figure A.2: Flame position in simulation result with TFC-model, represented by the product formation rate. Red indicates formation rates of 3000s^{-1} and higher. The inner inlet diameter is 38mm.

A.2 Additional plots

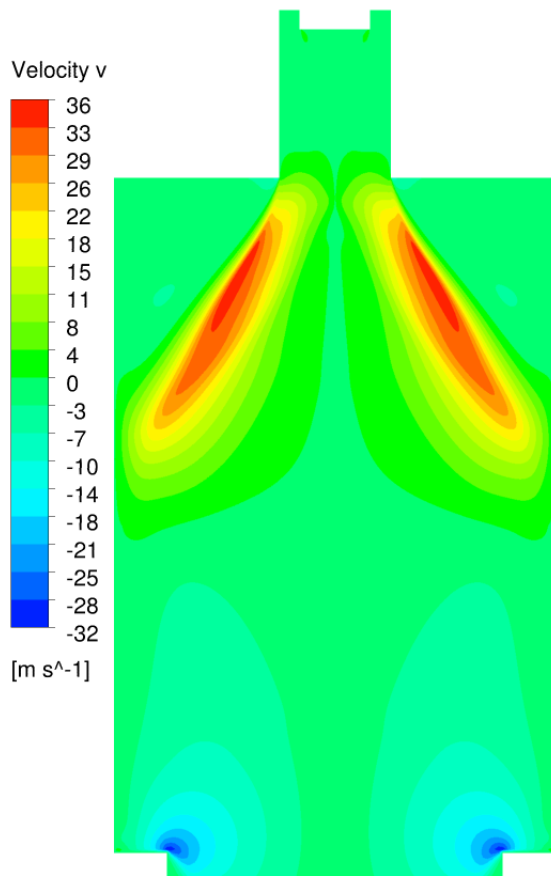


Figure A.3: TFC-model. Radial velocity plot.

A.2 Additional plots

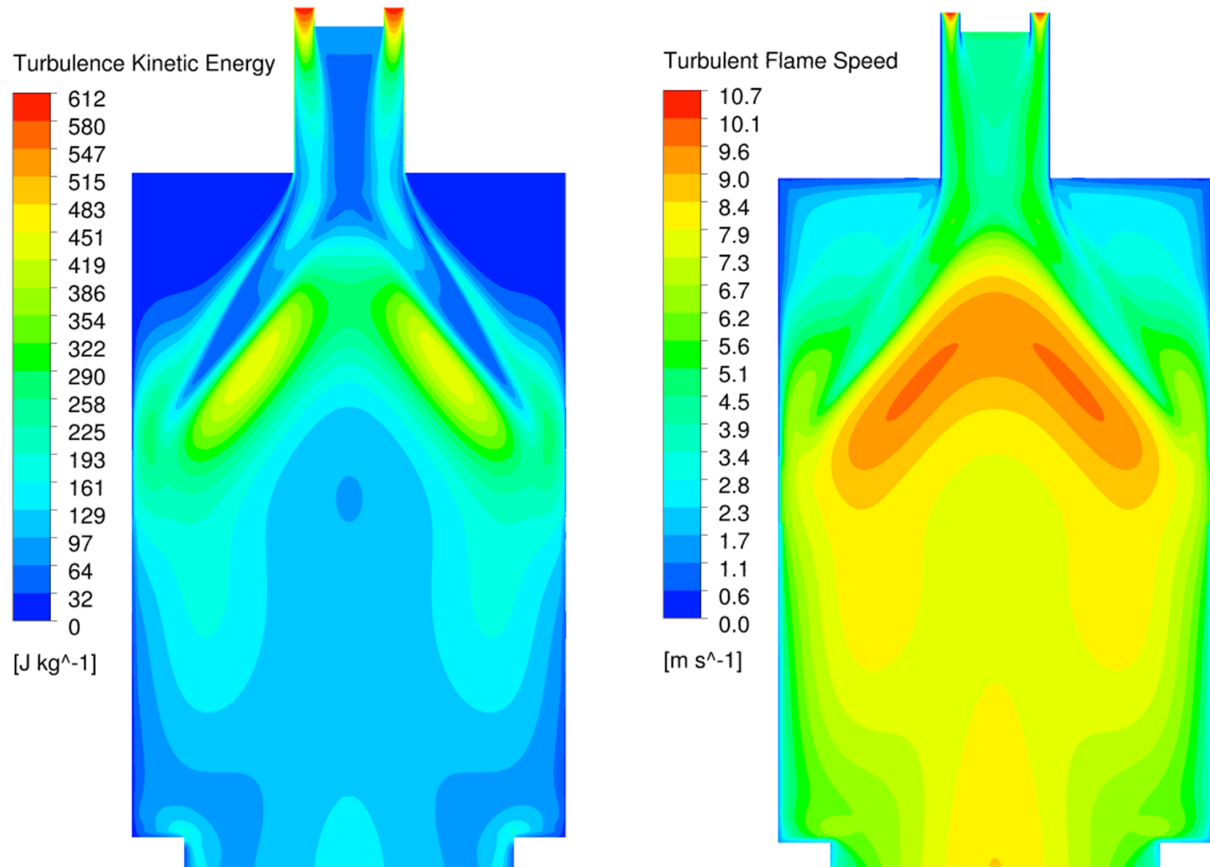


Figure A.4: TFC-model. Left side: Turbulence Kinetic Energy. Right side: Modeled turbulent flame speed

A.3 Additional information

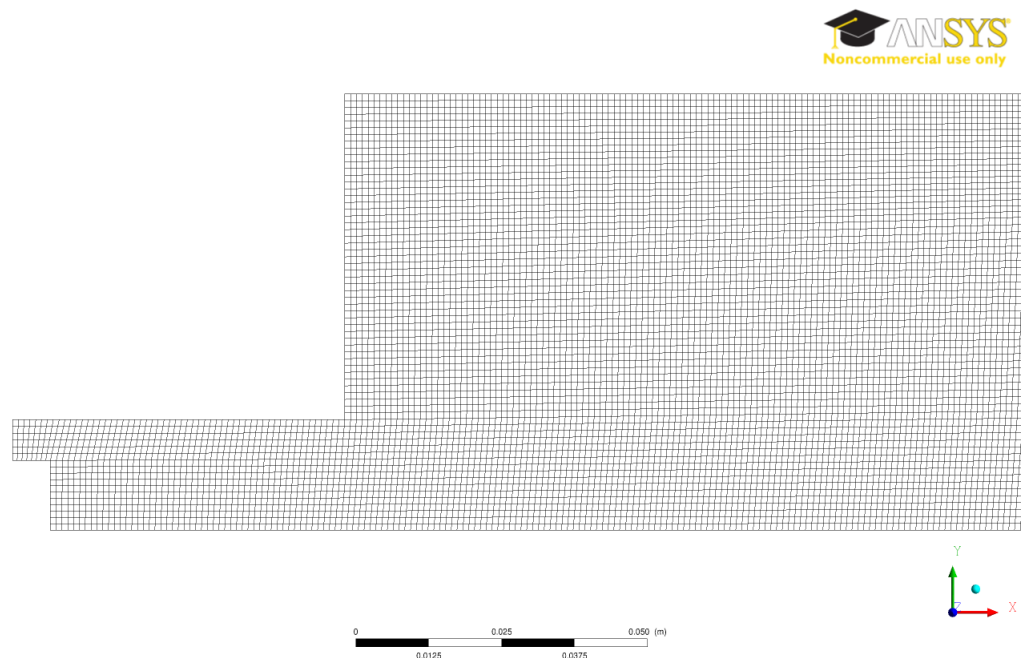


Figure A.5: Detail of the base mesh in the area of the injector.

A.3 Additional information

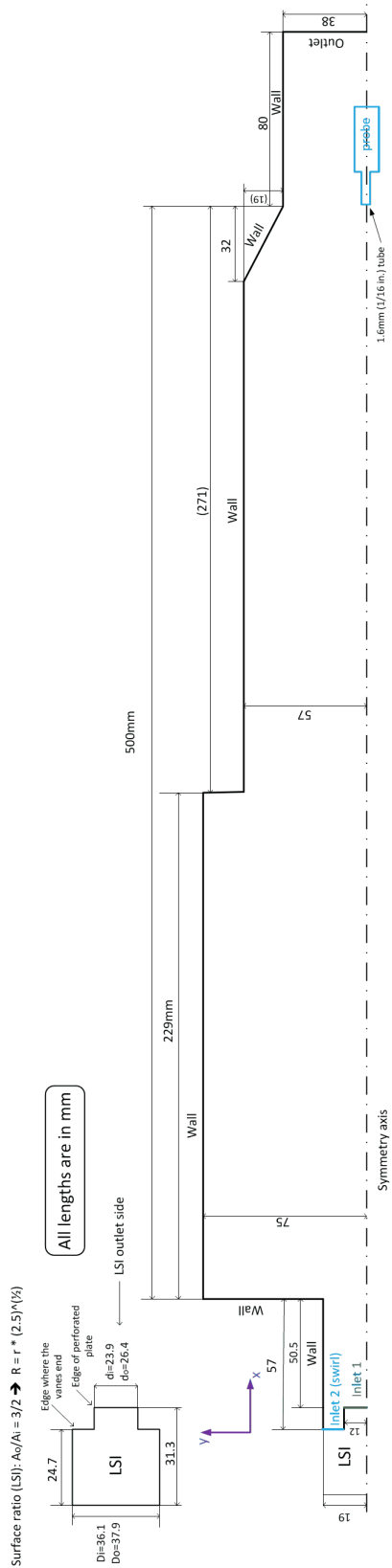


Figure A.6: Drawing of the simulation domain (combustion chamber) with all dimensions.

A.3 Additional information

Setup and boundary conditions of simulations

(non reacting)

Standard pressure	p_{stand}	Pa	101350
Standard Temperature	T_{stand}	K	294 (=70°F)
operating pressure	p_{out}	Pa	0
pressure in combustion chamber (specified at Outlet in Simulations)	p_{int}	atm.	4
Molar weight of air	M	kg/kmol	28.96
Universal Gas Constant	R_u	J/(kmol K)	8.31E+03
Volume flow rate	V	scfm	303.5
		scf/s	5.058
Volume flow (actual cubic ft/sec)		ft^3/s	1.948
$1 \text{ ft}^2 = 0.02831685 \text{ m}^2$		m^3/s	0.055
total mass flow rate	m_{tot}	kg/s	0.1720
Temperature at Inlets	T	K	453
Density of dry air (T at Inlet)	ρ_{air}	kg/m^3	3.117155
dynamic viscosity	η_{air}	kg/(sm)	2.496E-05
Isotropic Exponent	K		1.4
specific Gas Constant for air	R_{air}	J/(kgK)	287
Diameter of Inlet	d	m	0.038
Total area of Inlet	A_{inlet}	m^2	1.13E-03
Average velocity downstr. of LSI	U_0	m/s	48.65
Ratio of radii (LSI)	R_{LSI}		0.63
Ratio of mass flow rates (LSI)	m_{LSI}		0.33

	Inlet 1	Inlet 2 (swirl)
--	---------	-----------------

Radius	r	m	1.20E-02	1.90E-02
Area (3D)	A	m^2	4.52E-04	6.82E-04
Area of flow	A_h	m^2	1.33E-04	3.97E-04
Hydraulic diameter	d_h	m	2.40E-02	1.40E-02
Temperature	T	K	453	453
mass flow rate ratio (Bernoulli calc.)			0.25	0.75
mass flow rate (Bernoulli calc.)	m	kg/s	0.04299	0.12898
alternative mass flow ratio 1			0.20	0.80
alternative mass flow rate 1		kg/s	0.03440	0.13758
alternative mass flow ratio 2			0.225	0.775
alternative mass flow rate 2		kg/s	0.03870	0.13328
swirl vane angle	α	°		37
swirl angle (flow)	α	°		35
Swirl number (0.4 < S < 0.55)	S			0.50
velocity	c	m/s	30.49	74.10
axial velocity component	u		1	0.8192
		m/s	30.49	60.70
tangential velocity component	w		0	0.5736
		m/s	0	42.50
Mach number	Ma		0.071	0.174

Figure A.7: Raw data of simulation setup: Cold Flow at 4 atm. (part 1 of 2)

A.3 Additional information

kinematic viscosity air (T at Inlet)	v	m^2/s	8.01E-06	8.01E-06
char. Length for Re number	L	m	2.60E-03	7.00E-03
Reynolds number	Re		9900	64776
Char. Lengthscale for turbulence	L_t	m	0.0026	0.007
Turbulent Intensity (calc. with Re)	L_t		0.0507	0.0401

$[L_t = 0.16 * Re^{-1/8}]$

total pressure loss over LSI	Δp	psi	1.9	
		Pa	13100	
Bernoulli approach:				
$m = Cd * A * (2 * \rho * \Delta p)^{0.5}$	c_B	m/s	91.7	91.7
	m_B	kg/s	0.0379	0.1135
Total mass flow rate (Bernoulli)	$m_{tot,B}$	kg/s	0.1515	
<i>Comparison</i>				
mass flow rate ratio (Bernoulli)			0.1720	
			0.2504	0.7496

Figure A.8: Raw data of simulation setup: Cold Flow at 4 atm. (part 2 of 2)

A.3 Additional information

Setup and boundary conditions of simulations

Reacting CH4 (Case C-7 in D. Beerer's PhD thesis)

"Incompressible Flow"			
Standard pressure	p_{stand}	Pa	101350
Standard temperature	T_{stand}	K	294 (=70°F)
Pressure in combustion chamber (specified at Outlet in simulations)	p_{int}	atm.	4.11
		Pa	416136
Temperature at Inlet	T_{inlet}	K	418.49
Molar weight of air	M_{air}	kg/kmol	28.96
Molar weight of Methane	M_{CH_4}	kg/kmol	16.03
Universal Gas Constant	R_u	J/(kmol K)	8314.3
Volume flow rate	V	scfm	328.51
		scf/s	5.475
Volume flow rate (actual cubic ft/sec)		ft^3/s	1.898
$1 \text{ ft}^2 = 0.02831685 \text{ m}^2$		m^3/s	0.054
Mass flow rate air	m_{air}	kg/s	0.1862
Lower Heating Value of methane	LHV	MJ/kg	50
Heat release during combustion	Q	kW	386.7
Total area of heat losses	A_{heat}	m^2	0.223
Equivalence Ratio	ϕ		0.7146
"Luftzahl" $\lambda = 1/\phi$	λ		1.3994
Stoichiometric Air-Fuel Ratio	(A/F) _{st}		17.20
Air-Fuel Ratio	(A/F)		24.07
Mixture Fraction	f		0.0288
Mass flow rate Methane	m_{CH_4}	kg/s	0.0077
Total mass flow rate	m_{tot}	kg/s	0.1939
Mass fraction air	Y_{air}		0.9601
<hr/>			
<i>Fresh gas</i>			
Mass fraction Oxygen	Y_{O_2}		0.2016
Mass fraction Nitrogen	Y_{N_2}		0.7585
Mass fraction Methane	Y_{CH_4}		0.0399
Adiabatic Flame Temperature	T_{ad}	K	1950
(Calculation Program TUM)			
<i>Exhaust gas</i>			
Mass fraction Oxygen	Y_{O_2}		0.0639
Mass fraction Nitrogen	Y_{N_2}		0.7364
Mass fraction CO2	Y_{CO_2}		0.1099
Mass fraction H2O	$Y_{\text{H}_2\text{O}}$		0.0899
<hr/>			
Density of dry air (T at Inlet)	ρ_{air}	kg/m^3	3.464
Dynamic viscosity of air	η_{air}	kg/(sm)	2.358E-05
Isotropic exponent	κ		1.4
Specific gas constant for air	R_{air}	J/(kgK)	287
Diameter of Inlet	d	m	0.038
Total area of Inlet	A_{inlet}	m^2	1.13E-03
Average velocity in injector	U_0	m/s	49.4
Ratio of radii (LSI for calculation of S_N)	R_{LSI}		0.63
Ratio of mass flow rates (----"----)	m_{LSI}		0.29

Figure A.9: Raw data of simulation setup: Hot Flow at 4 atm. (part 1 of 3)

A.3 Additional information

Damköhler Number	Da		0.638
Karlovitz Number	Ka		31.4
Laminar Flame Speed	S_l	m/s	0.2307
Turbulent Flame Speed	S_t	m/s	11.77
Lift off height	x_f	mm	7
Thermal conductivity	k	W/mK	0.03489
Thermal diffusivity	α	m^2/s	9.91E-06
Specific heat capacity	c_p	J/(kgK)	1016

			Inlet 1 (center)	Inlet 2 (swirl)
Radius	R	m	1.20E-02	1.90E-02
Area (3D)	A	m^2	4.52E-04	6.82E-04
Area of flow	A_{Flow}	m^2	1.33E-04	3.97E-04
Hydraulic diameter	d_h	m	2.40E-02	1.40E-02
Temperature	T	K	418	418
Mass flow rate ratio			0.225	0.775
Mass flow rate	m	kg/s	0.04363	0.15027
swirl vane angle	α	°		37
Swirl angle (flow)	α	°		35
Swirl number	S_N			0.52
Velocity vector	c	m/s	27.8	77.7
Axial velocity component	U		1	0.8192
		m/s	27.8	63.6
Tangential velocity component	W		0	0.5736
		m/s	0	44.56
Mach number	Ma		0.068	0.189
Axial velocity (in experiment)	u_{Exp}	m/s	94.9	109.2
Kinematic viscosity air (T at Inlet)	v	m^2/s	6.81E-06	6.81E-06
Char. Length for Re number	L	m	2.60E-03	7.00E-03
Reynolds number	Re		10633	79882
Char. Lengthscale for turbulence	L_t	m	0.0024	0.0070
Turbulent Intensity (calc. with Re)	I_t		0.050	0.039
[$I_t = 0.16 * Re^{-1/8}$]				
Turbulent Intensity (Exp data)		u'/U	0.26	0.26

total pressure loss over LSI	Δp	psi	2.54
		Pa	17513
Bernoulli approach $m = Cd * A * (2 * \rho * \Delta p)^{0.5}$			
	c_B	m/s	100.6
	m_B	kg/s	0.0462
Total mass flow rate (Bernoulli)	$m_{tot,B}$	kg/s	0.1846
Comparison			0.1939
mass flow rate ratio (Bernoulli)			0.2504
			0.7496

Figure A.10: Raw data of simulation setup: Hot Flow at 4 atm. (part 2 of 3)

A.3 Additional information

Heat Losses

(Fully developed turbulent pipe flow)

Diameter of pipe	d	m	0.15
Length of pipe	L	m	0.5
Total surface area	A	m^2	0.236
axial velocity	U	m/s	14.8
density of hot gas	ρ	kg/m^3	0.74
dynamic viscosity	η	$kg/(sm)$	6.00E-05
kinematic viscosity	v	m^2/s	8.07E-05
specific heat capacity	cp	J/(kgK)	1244
Thermal conductivity air	k_{air}	W/(mK)	0.10
Reynolds-number	Re		2.74E+04
Prandtl-number	Pr		0.73
Nusselt-number	Nu		66.8
heat transfer coefficient	h	W/(m^2K)	45.5
heat transfer coefficient corrected			136.6 (factor 3)
heat flux (max value)	q	W/ m^2	209278
Total heat loss	Q	kW	49.3
		%	12.8

Figure A.11: Raw data of simulation setup: Hot Flow at 4 atm. (part 3 of 3)

Bibliography

- [1] Combustion calculation program, method 2 (“verbrennungsberechnung methode 2”). http://www.td.mw.tum.de/tum-td/de/studium/lehre/thermo_2/download/, April 2013.
- [2] N. A. Adams. *Turbulente Strömungen*. Lehrstuhl für Aerodynamik, Technische Universität München, 2008.
- [3] D. Beerer. *Combustion characteristics and performance of Low-Swirl Injectors with natural gas and alternative fuels at elevated pressures and temperatures*. PhD thesis, University of California, Irvine, 2013.
- [4] R. K. Cheng and D. Littlejohn. Effects of combustor geometry on the flowfields and flame properties of a low swirl injector. In *Proceedings of ASME Turbo Expo 2008: Power for Land, Sea and Air*, 2008.
- [5] L. Tay Wo Chong, T. Komarek, M. Zellhuber, J. Lenz, C. Hirsch, and W. Polifke. Influence of strain and heat loss on flame stabilization in a non-adiabatic combustor. In *Proceedings of the European Combustion Meeting*, 2009.
- [6] Marc Day, Shigeru Tachibana, John Bell, Michael Lijewski, Vince Beckner, and Robert Cheng. A combined computational and experimental characterization of lean premixed turbulent low swirl laboratory flames. i. methane flames. Technical report, Lawrence Berkeley National Laboratory, Berkeley, CA, USA, 2012.
- [7] A. Fiskum. Calculation of nox formation in a swirl burner. Master’s thesis, Norwegian University of Science and Technology, Trondheim, Norway, 2008.
- [8] ANSYS Inc. Ansys fluent theory guide, release 14.0, November 2011.
- [9] ANSYS Inc. Ansys fluent user’s guide, release 14.0, November 2011.
- [10] M. Karalus, B. Fackler, I. Novoselov, J. Kramlich, and P. Malte. Characterizing the mechanism of lean blowout for a recirculation-stabilized premixed hydrogen flame. In *Proceedings of ASME Turbo Expo 2012*, 2012.
- [11] H. Pitsch. Enabling advanced modeling and simulations for fuel-flexible combustors. Technical report, Department of Mechanical Engineering, Stanford University, 2010. <http://www.osti.gov/bridge/servlets/purl/1001422-CUoe54/1001422.pdf>.

BIBLIOGRAPHY

- [12] O. Spangelo. *Experimental and theoretical studies of a low NO_x swirl burner*. PhD thesis, Norwegian University of Science and Technology, Trondheim, Norway, 2004.
- [13] Stephen R. Turns. *An Introduction to Combustion*. Mc Graw Hill, 2000.